

# Chapter 14

## Description of Core-Ionized and Core-Excited States by Density Functional Theory and Time-Dependent Density Functional Theory

Yutaka Imamura and Hiromi Nakai

**Abstract** This chapter discusses descriptions of core-ionized and core-excited states by density functional theory (DFT) and by time-dependent density functional theory (TDDFT). The core orbitals are analyzed by evaluating core-excitation energies computed by DFT and TDDFT; their orbital energies are found to contain significantly larger self-interaction errors in comparison with those of valence orbitals. The analysis justifies the inclusion of Hartree-Fock exchange (HFx), capable of reducing self-interactions, and motivates construction of hybrid functional with appropriate HFx portions for core and valence orbitals. The determination of the HFx portions based on a first-principle approach is also explored and numerically assessed.

### 14.1 Introduction

Kohn-Sham density functional theory (KS-DFT) [1–4] has been established as a computational tool for estimating physical properties of ground states such as standard enthalpies of formation, because of the cost-effective performance. The establishment of KS-DFT was achieved by development of exchange-correlation (XC) functionals such as the local density approximation (LDA) [5, 6], generalized gradient approximation (GGA) [7–9], meta-GGA [10], global hybrid [11–13], and long-range corrected (LC) and short-range corrected hybrid [14–18] functionals. Although long-standing KS-DFT deficiencies such as the lack of van der Waals interaction in XC functionals were pointed out in 2000s, the recipes for overcoming the deficiencies have been proposed [19–23] and largely removed those deficiencies.

---

Y. Imamura • H. Nakai (✉)

Department of Chemistry and Biochemistry, School of Advanced Science and Engineering,  
Waseda University, Tokyo 169-8555, Japan  
e-mail: [nakai@waseda.jp](mailto:nakai@waseda.jp)

In addition to the descriptions of ground states, excited states have been also computed by time-dependent density functional theory (TDDFT) [24–28]. Valence-excitation energies are accurately estimated without exhibiting a tendency of overestimation, which is typically confirmed for configuration interaction singles (CIS) calculations [28]. TDDFT has been plagued by the underestimation of the charge-transfer (CT) and Rydberg excitation energies owing to the lack of the long-range Coulomb interaction [29, 30]. The recently proposed and widely accepted LC functional [15] alleviates the obstacle and is a powerful tool for practical applications.

Although DFT and TDDFT have been utilized for describing valence orbitals in the ground and excited states, description of core orbitals still needs to be theoretically and numerically investigated because of the peculiar localized distributions of core electrons. Core electrons provide important information regarding molecular structure and dynamics through X-ray photoabsorption and electron energy loss spectra. Numerous theoretical attempts to describe core orbitals [31–62] have been proposed. Green function [31–33] and wave function [34–36] approaches including recent studies by the symmetry adapted cluster configuration interaction (SAC-CI) [34] and multiconfigurational self-consistent-field multireference perturbation theory (MCSCF-MRPT) [35] have been reported. However, this chapter focuses on DFT-based approaches. See a good review on this matter [37] in more details if you are interested.

In DFT, transition potential [38–42] and  $\Delta$ self-consistent field ( $\Delta$ SCF) [42–44] have been major methodologies for describing core orbitals. They offer relatively accurate descriptions for core orbitals, but their applicabilities are limited by symmetries because the desired state cannot be necessarily produced by specifying occupation numbers. TDDFT with the van Leeuwen-Baerends 94 (LB94) functional [45, 57, 58] was reported. However, more extensive studies on core orbitals by DFT and TDDFT have been demanded, and a great number of other developments in the framework of DFT and TDDFT have progressed [46–62].

This chapter describes our several attempts [46–56] to accurately describe core orbitals in the DFT approach. Section 14.2 analyzes CO core orbitals for core-excitation energies in terms of self-interaction. Section 14.3 explains the core-valence Becke-three-Lee-Yang-Parr (CV-B3LYP) functional [50–52] including Hartree-Fock exchange (HFX) portions designed to reproduce valence as well as core-excitation energies. Section 14.4 reviews orbital-specific (OS) functionals [53–56] that are considered as an extension of CV-B3LYP. Finally, general conclusions are addressed.

## 14.2 Analysis of Core Orbitals

Description of core orbitals is investigated by estimating core-excitation energies of carbon monoxide, computed by the self-interaction corrected (SIC)- $\Delta$ SCF and SIC-TDDFT methods. First, the formulations of SIC- $\Delta$ SCF and SIC-TDDFT are briefly introduced, and subsequently numerical analysis is demonstrated.

## 14.2.1 Theoretical Aspects

### 14.2.1.1 SIC-ΔSCF

The excitation energy by the ΔSCF method is given as follows:

$$\omega^{\Delta\text{SCF}}(i_\sigma \rightarrow a_\sigma) = E_{\text{ES}}(\Psi_{i_\sigma}^{a_\sigma}) - E_{\text{GS}}(\Psi_0). \quad (14.1)$$

The spatial orbital indices  $\{i, j, \dots\}$ ,  $\{a, b, \dots\}$ , and  $\{p, q, \dots\}$  are used for the occupied, unoccupied, and general orbitals, respectively.  $\sigma$  and  $\tau$  denote spins.  $E_{\text{GS}}(\psi_0)$  is the ground-state energy, and  $E_{\text{ES}}(\psi_{i_\sigma}^{a_\sigma})$  is the  $i_\sigma \rightarrow a_\sigma$  excited-state energy, which is calculated self-consistently in the spin-unrestricted formalism with the constraint that the occupation numbers of orbitals  $i_\sigma$  and  $a_\sigma$  are 0 and 1, respectively. In the ΔSCF method, the difference of total energies plays an essential role in determining excitation energies.

The Perdew-Zunger or one-electron self-interaction error in the ΔSCF method is written as [63]

$$E^{\text{SIE}} = \sum_{i,\sigma} E_{\text{xc}}[\rho_{i_\sigma}, 0] + J[\rho_{i_\sigma}], \quad (14.2)$$

where  $E_{\text{xc}}$  and  $J$  represent an XC functional and Coulomb interaction, respectively. When the exact XC functional, that is, self-interaction-free (SIF) functional, is used, the following relation automatically holds:

$$E^{\text{SIE}} = 0. \quad (14.3)$$

The SIC total energy is simply defined as

$$E^{\text{SIC}} = E - E^{\text{SIE}}. \quad (14.4)$$

The SIC excitation energy by the ΔSCF method is estimated as

$$\omega^{\text{SIC}-\Delta\text{SCF}}(i_\sigma \rightarrow a_\sigma) = E_{\text{ES}}^{\text{SIC}}(\Psi_{i_\sigma}^{a_\sigma}) - E_{\text{GS}}^{\text{SIC}}(\Psi_0), \quad (14.5)$$

where  $E_{\text{GS}}^{\text{SIC}}(\psi_0)$  and  $E_{\text{ES}}^{\text{SIC}}(\psi_{i_\sigma}^{a_\sigma})$  are the SIC total energies of the ground and  $i_\sigma \rightarrow a_\sigma$  excited states, respectively. In the study all Perdew-Zunger SIEs are estimated in a post-SCF manner.

### 14.2.1.2 SIC-TDDFT

The excitation energies  $\omega$  for TDDFT are computed by solving the following non-Hermitian eigenvalue equation [25–28]:

$$\begin{pmatrix} A & B \\ B^* & A^* \end{pmatrix} \begin{pmatrix} X \\ Y \end{pmatrix} = \omega^{\text{TDDFT}} \begin{pmatrix} 1 & 0 \\ 0 & -1 \end{pmatrix} \begin{pmatrix} X \\ Y \end{pmatrix}. \quad (14.6)$$

The matrix elements in Eq. (14.6) are given by

$$A_{ai\sigma,bj\tau} = \delta_{ij}\delta_{ab}\delta_{\sigma\tau}(\varepsilon_{a\sigma} - \varepsilon_{i\tau}) + (a_{\sigma}i_{\sigma}|j_{\tau}b_{\tau}) - c_{\text{HF}}\delta_{\sigma\tau}(a_{\sigma}b_{\tau}|j_{\tau}i_{\sigma}) \\ + c_{\text{DFT}}(a_{\sigma}i_{\sigma}|w_{\sigma\tau}|j_{\tau}b_{\tau}) \quad (14.7)$$

and

$$B_{ai\sigma,bj\tau} = (a_{\sigma}i_{\sigma}|b_{\tau}j_{\tau}) - c_{\text{HF}}\delta_{\sigma\tau}(a_{\sigma}j_{\tau}|b_{\tau}i_{\sigma}) + c_{\text{DFT}}(a_{\sigma}i_{\sigma}|w_{\sigma\tau}|b_{\tau}j_{\tau}), \quad (14.8)$$

where  $c_{\text{HF}}$  and  $c_{\text{DFT}}$  represent portions of HFX and DFT XC functional, respectively. The  $w$  term is given by

$$(p_{\sigma}q_{\sigma}|w_{\sigma\tau}|r_{\tau}s_{\tau}) = \int d\mathbf{r}d\mathbf{r}'\phi_{p\sigma}^*(\mathbf{r})\phi_{q\sigma}(\mathbf{r})\frac{\delta^2 E_{\text{xc}}}{\delta\rho_{\sigma}(\mathbf{r})\delta\rho_{\tau}(\mathbf{r}')}\phi_{r\tau}^*(\mathbf{r}')\phi_{s\tau}(\mathbf{r}'), \quad (14.9)$$

where  $\phi$  represents a KS orbital. In this method, the difference of orbital energies is the key for estimating excitation energies.

The Perdew-Zunger SIE for an occupied orbital energy can be defined in a way similar to Ref. [63]:

$$\varepsilon_{i\sigma}^{\text{SIE}} = J[\rho_{i\sigma}] + (i_{\sigma}|V_{\text{xc}}[\rho_{i\sigma}]|i_{\sigma}), \quad (14.10)$$

where  $V_{\text{xc}}$  represents the XC potential. If the exact XC functional is used,  $\varepsilon_{i\sigma}^{\text{SIE}} = 0$  for each occupied orbital. Here, the SIC occupied orbital energy is defined as follows:

$$\varepsilon_{i\sigma}^{\text{SIC}} = \varepsilon_{i\sigma} - \varepsilon_{i\sigma}^{\text{SIE}}. \quad (14.11)$$

For unoccupied orbitals, the SIE should be defined in a different fashion; once an electron excites from the occupied orbital  $i$  to the unoccupied orbital  $a$ , the SIE can be defined as follows:

$$\varepsilon_{a\sigma}^{\text{SIE}}(i \rightarrow a) = c_{\text{HF}}J_{ia\sigma} + K_{ia\sigma} + c_{\text{DFT}}(i_{\sigma}a_{\sigma}|w_{\text{xc}}|i_{\sigma}a_{\sigma}). \quad (14.12)$$

In time-dependent Hartree-Fock (TDHF) and TDDFT calculations, the self-interactions for unoccupied orbitals are automatically corrected. Here, in order to remove the SIEs of occupied orbitals, the following modified  $\mathbf{A}$  matrix is adopted to estimate SIC core-excitation energies:

$$A_{ai\sigma,bj\tau}^{\text{SIC}} = \delta_{ij}\delta_{ab}\delta_{\sigma\tau}(\varepsilon_{a\sigma} - \varepsilon_{i\tau}^{\text{SIC}}) + (a_{\sigma}i_{\sigma}|j_{\tau}b_{\tau}) - c_{\text{HF}}\delta_{\sigma\tau}(a_{\sigma}b_{\tau}|j_{\tau}i_{\sigma}) \\ + c_{\text{DFT}}(a_{\sigma}i_{\sigma}|w_{\sigma\tau}|j_{\tau}b_{\tau}). \quad (14.13)$$

The combination of Eq. (14.8) with Eq. (14.13) leads to SIC core-excitation energies. In this study, all Perdew-Zunger SIEs are estimated in a post-SCF manner.

## 14.2.2 Analysis on Self-Interaction of Core Electrons

In this chapter, the Perdew-Zunger SIEs of the CO molecule were calculated in the KS-DFT scheme with Becke-Lee-Yang-Parr (BLYP) [7, 8], B3LYP [11, 12], and Becke-Half-and-Half-Lee-Yang-Parr (BHHLYP) [64] functionals. Since the LYP functional is SIF, the SIEs of BLYP and BHHLYP come from an approximate exchange functional: Becke88 (B88) [7]. The correlation part of B3LYP consists of LYP (nonlocal part) [8] and Vosko-Wilk-Nusair (VWN) (local part) [6], which is not SIF. The main contribution of SIEs is still from the B88 exchange functional because the magnitude of the correlation part of B3LYP is relatively small. The cc-pCVTZ basis set [65, 66] combined with the Dunning-Hay basis functions [67] was adopted. 6d and 10f basis functions were used. Since SIEs cannot be invariant under unitary transformations, degenerate orbitals of  $2p\pi$  and  $2p\pi^*$  are designed to be fixed on the  $x$ - and  $y$ -axes where the  $z$ -axis is the CO-bonding direction. The coordinates of CO molecule were optimized at the B3LYP/cc-pVTZ [65] level. Calculations were carried out in the Gaussian 03 suite of programs [68].

### 14.2.2.1 Comparison Between $\Delta$ SCF and SIC- $\Delta$ SCF

The SIEs for total energies given in Eq. (14.3) are examined, which play the key role in the  $\Delta$ SCF method. Table 14.1 lists SIEs of total and respective orbitals for the CO ground and excited states such as  $C1s \rightarrow \pi^*$ ,  $C1s \rightarrow 3s$ ,  $O1s \rightarrow \pi^*$ , and  $O1s \rightarrow 3s$  states, respectively. The total SIEs are negative for the ground and excited states. For the ground state, the SIEs for BLYP, B3LYP, and BHHLYP are  $-14.89$ ,  $-11.30$ , and  $-7.24$  eV, respectively. For the excited states, the SIEs have slightly larger negative values. The C and O  $1s \rightarrow \pi^*$  SIEs tend to be slightly larger than those of C and O  $1s \rightarrow 3s$  excitations. The total SIEs increase for not only the ground state but also excited states according to the order of functional: BHHLYP, B3LYP, and BLYP, which is consistent with the HFx portions. This behavior can be explained by the exact cancellation between HFx and Coulomb interaction.

Next, the SIEs to core and valence orbitals are examined. The sign of SIEs depends on orbital type, namely, they are positive for core orbitals and negative for valence orbitals. Error cancellation occurs if core and valence orbitals are occupied. However, if an electron excites from a core orbital to an unoccupied orbital, SIEs may increase by reduction of error cancellation. As shown in Table 14.1, the total SIEs of the excited states have larger negative values than that of the ground state. For example, the total SIEs of BLYP is  $-14.89$  eV for the ground state and  $-17.80$  eV for the  $C1s \rightarrow 2p\pi^*$  state.

Table 14.2 summarizes CO core-excitation energies calculated by the  $\Delta$ SCF and SIC- $\Delta$ SCF methods using HF and KS-DFT with BLYP, B3LYP, and BHHLYP.

**Table 14.1** SIEs of  $\Delta$ SCF calculations for the CO molecule at DFT/cc-pCVTZ with the Dunning-Hay basis functions in eV

Functional	State	Core (C)	Core (O)	Valence <sup>a</sup>	Total
BLYP	Ground state	0.76	0.48	-16.14	-14.89
	C1s $\rightarrow$ 2p $\pi^*$	0.50	0.48	-18.78	-17.80
	C1s $\rightarrow$ 3s	0.50	0.49	-17.79	-16.80
	O1s $\rightarrow$ 2p $\pi^*$	0.76	0.37	-20.51	-19.38
	O1s $\rightarrow$ 3s	0.76	0.37	-19.15	-18.03
B3LYP	Ground state	1.30	0.77	-13.38	-11.30
	C1s $\rightarrow$ 2p $\pi^*$	0.77	0.77	-15.44	-13.90
	C1s $\rightarrow$ 3s	0.77	0.78	-14.69	-13.15
	O1s $\rightarrow$ 2p $\pi^*$	1.30	0.51	-16.92	-15.11
	O1s $\rightarrow$ 3s	1.31	0.51	-15.88	-14.06
BHHLYP	Ground state	0.40	0.27	-7.91	-7.24
	C1s $\rightarrow$ 2p $\pi^*$	0.26	0.27	-9.23	-8.70
	C1s $\rightarrow$ 3s	0.26	0.27	-8.74	-8.22
	O1s $\rightarrow$ 2p $\pi^*$	0.40	0.19	-10.20	-9.60
	O1s $\rightarrow$ 3s	0.40	0.19	-9.48	-8.88

<sup>a</sup>For Rydberg excitations, SIEs of valence and Rydberg orbitals are evaluated

**Table 14.2** CO core-excitation energies by  $\Delta$ SCF using DFT/cc-pCVTZ with the Dunning-Hay basis functions in eV

Transition	BLYP		B3LYP		BHHLYP		HF	Expt.
	$\Delta$ SCF	SIC- $\Delta$ SCF	$\Delta$ SCF	SIC- $\Delta$ SCF	$\Delta$ SCF	SIC- $\Delta$ SCF		
C1s $\rightarrow$ 2p $\pi^*$	286.36	290.85	286.47	290.27	287.02	289.39	287.14	287.4 <sup>a</sup>
	(-1.04)	(3.45)	(-0.93)	(2.87)	(-0.38)	(1.99)	(-0.26)	
C1s $\rightarrow$ 3s	292.26	295.39	292.62	295.38	293.46	295.10	293.90	292.37 <sup>b</sup>
	(-0.11)	(3.02)	(0.25)	(3.01)	(1.09)	(2.73)	(1.53)	
O1s $\rightarrow$ 2p $\pi^*$	533.55	536.45	533.33	535.92	533.66	535.12	533.14	534.2 <sup>a</sup>
	(-0.65)	(2.25)	(-0.87)	(1.72)	(-0.54)	(0.92)	(-1.06)	
O1s $\rightarrow$ 3s	538.34	540.25	538.29	540.14	538.77	539.74	538.94	538.8 <sup>c</sup>
	(-0.46)	(1.45)	(-0.51)	(1.34)	(-0.03)	(0.94)	(0.14)	

<sup>a</sup>Ref. [40]

<sup>b</sup>Ref. [69]

<sup>c</sup>Ref. [70]

The deviations from experimental values are shown in parentheses. Core-excitation energies of the  $\Delta$ SCF and SIC- $\Delta$ SCF methods do not differ greatly in spite of the large SIEs in Table 14.1. The reason is that SIE cancellation occurs between SIEs of the ground and excited states. The  $\Delta$ SCF and SIC- $\Delta$ SCF methods provide considerably smaller deviations than TDHF because they are capable of incorporating orbital relaxation [46], which is considered one of the main sources of errors in TDHF calculations. For core  $\rightarrow$  Rydberg and core  $\rightarrow$  valence excitations, the  $\Delta$ SCF method with KS-DFT tends to slightly underestimate excitation energies, while the SIC- $\Delta$ SCF method with KS-DFT overestimates. The deviations of the  $\Delta$ SCF method are smaller than those of the SIC- $\Delta$ SCF method, which is supposed

to yield accurate excitation energies because it satisfies the physical condition: no self-interaction. However, this is not the case. The B88 exchange functional was constructed on the assumption that total energy of the B88 exchange has the SIE. Thus, if the SIE is removed from the total energies, the balance may be lost in the  $\Delta$ SCF calculations.

As is widely known, KS-DFT succeeds in reproducing standard enthalpies of formation of the small G2 set within 3–7 kcal/mol with commonly used functionals [71]. Since the  $\Delta$ SCF method estimates excitation energies from total energies of two different states, the accuracy for the core-excitation energies is predictable.

#### 14.2.2.2 Comparison Between TDDFT and SIC-TDDFT

The SIEs are examined for orbital energies, which play the key role in TDDFT. Table 14.3 shows the SIEs of CO occupied orbital energies for BLYP, B3LYP, and BHHLYP. The HF result is omitted because HF occupied orbitals are SIF. All SIEs are positive for all functionals. In particular, the SIEs of BLYP are 47.55 and 35.06 eV for C and O 1s orbitals, respectively. As HFx portions increase, SIEs decrease: BHHLYP and B3LYP give approximately 0.5 and 0.8 times the values of the BLYP SIEs for O 1s and C 1s orbitals, respectively. Compared with those of core orbitals, the SIEs of valence orbitals are significantly smaller: the SIEs of  $2p\pi$  and  $2p\sigma$  are 3.33 and 4.40 eV for BLYP. B3LYP does not give approximately 0.8 times the value of BLYP SIEs for  $2p\pi$  and  $2p\sigma$ .

Table 14.4 shows SIEs for CO unoccupied orbital energies. These SIEs defined in Eq. (14.12) are calculated by TDHF and TDDFT with BLYP, B3LYP, and BHHLYP. TDDFT with BLYP gives small SIEs for all cases, while SIEs decrease as HFx portion decreases. For example, the SIEs for  $C1s \rightarrow 2p\pi^*$  are 6.76, 5.37, 3.13, and

**Table 14.3** SIEs of orbital energies for the CO molecule at DFT/cc-pVTZ with the Dunning-Hay basis functions in eV

	BLYP	B3LYP	BHHLYP
O1s	47.55	36.50	23.84
C1s	35.06	26.55	17.60
$2s\sigma$	7.63	5.01	3.81
$2s\sigma^*$	5.10	3.10	2.60
$2p\pi$	3.33	1.68	1.67
$2p\sigma$	4.40	2.65	2.31

**Table 14.4** SIEs of unoccupied orbital energies for the CO molecule at DFT/cc-pCVTZ with the Dunning-Hay basis functions in eV

Virtual orbital	Transition	BLYP	B3LYP	BHHLYP	TDHF
$2p\pi^*$	O1s $\rightarrow$ $2p\pi^*$	-0.06	2.83	5.07	6.92
	C1s $\rightarrow$ $2p\pi^*$	-0.03	3.13	5.37	6.76
3s	O1s $\rightarrow$ 3s	-0.02	0.93	2.14	9.46
	C1s $\rightarrow$ 3s	-0.02	0.89	2.07	10.95

**Table 14.5** Core-excitation energies calculated by TDDFT and SIC-TDDFT with cc-pCVTZ with the Dunning-Hay basis functions in eV

Transition	BLYP		B3LYP		BHHLYP		TDHF	Expt.
	TDDFT	SIC-TDDFT	TDDFT	SIC-TDDFT	TDDFT	SIC-TDDFT		
C1s $\rightarrow$ 2p $\pi^*$	271.29 (-16.11)	306.35 (18.95)	276.17 (-11.23)	302.71 (15.31)	283.55 (-3.85)	301.14 (13.74)	294.39 (6.99)	287.4 <sup>a</sup>
C1s $\rightarrow$ 3s	272.76 (-19.61)	307.81 (15.44)	279.40 (-12.97)	305.94 (13.57)	289.40 (-2.97)	307.00 (14.63)	304.68 (12.31)	534.2 <sup>a</sup>
O1s $\rightarrow$ 2p $\pi^*$	512.29 (-21.91)	559.84 (25.64)	519.82 (-14.38)	556.32 (22.12)	531.65 (-2.55)	555.49 (21.29)	550.10 (15.90)	292.37 <sup>b</sup>
O1s $\rightarrow$ 3s	513.78 (-25.02)	561.32 (22.52)	522.70 (-16.10)	559.20 (20.40)	536.39 (-2.41)	560.22 (21.42)	557.82 (19.02)	538.8 <sup>c</sup>

<sup>a</sup>Ref. [40]<sup>b</sup>Ref. [69]<sup>c</sup>Ref. [70]

-0.03 eV for TDHF and TDDFT with the BHHLYP, B3LYP, and BLYP functionals, respectively. Similarly, the SIEs for C1s  $\rightarrow$  3s are 10.95, 2.07, 0.89, and -0.02 eV, respectively. This trend is the opposite of occupied orbitals.

Table 14.5 lists CO core-excitation energies calculated by TDHF, TDDFT, and SIC-TDDFT with BLYP, B3LYP, and BHHLYP.  $\omega^{\text{SIC-TDDFT}}$  represents the excitation energies obtained by diagonalizing the non-Hermitian matrix composed of Eqs. (14.8) and (14.13). The deviations from experimental values are shown in parentheses. TDDFT and SIC-TDDFT with BLYP, B3LYP, and BHHLYP for core  $\rightarrow$  Rydberg and core  $\rightarrow$  valence show different behaviors; underestimation and overestimation for TDDFT and SIC-TDDFT, respectively. These results indicate that elimination of SIEs reverses the trend of the underestimation.  $\omega^{\text{TDDFT}}$  is strongly dependent on the XC functionals; for example, the TDDFT deviations for BLYP, B3LYP, and BHHLYP are -16.11, -11.23, and -3.85 eV for C1s  $\rightarrow$  2p $\pi^*$ , respectively. On the other hand,  $\omega^{\text{SIC-TDDFT}}$  is less dependent on them; for example, the SIC-TDDFT deviations for BLYP, B3LYP, and BHHLYP are 18.95, 15.31, and 13.74 eV, respectively. The core excitations from the O 1s orbital yield larger deviations than those from the C 1s orbital for SIC-TDDFT and TDHF, while hybrid TDDFT with a 50 % exchange, BHHLYP, provides core-excitation energies with a similar accuracy. These results indicate that SIC-TDDFT fails to yield accurate core-excitation energies and rather increases deviations despite no self-interaction.

### 14.2.3 Discussion

KS-DFT using self-interaction-contained XC functionals does not retain a relation between the total and orbital energies:

$$E = \sum_{i\sigma} \varepsilon_{i\sigma} - \frac{1}{2} \sum_{i\sigma, j\tau} \langle i_{\sigma} j_{\tau} || i_{\sigma} j_{\tau} \rangle, \quad (14.14)$$



which is satisfied for HF because Koopmans' theorem holds for HF but does not hold for DFT with self-interaction-contained XC functionals. Thus, the total energy and orbital energies are not directly correlated for self-interaction-contained XC functionals, which brings us to the fact that the Perdew-Zunger SIEs in orbital energies greatly differ from those in total energies as shown in the previous section.

Let us examine in greater detail how the SIEs of orbital energies and total energies differ for the Slater-Dirac exchange [5], with which the B88 exchange functional becomes equivalent for the homogeneous electron gas. A similar analysis has been performed previously [63]. The Slater-Dirac exchange is given by

$$E_x^{\text{Slater}} = - \sum_{\sigma} \int C_X \rho_{\sigma}^{4/3} d\mathbf{r}, \quad (14.15)$$

where  $C_X = (3/4) \sqrt[3]{6/\pi}$ . The self-interaction of the exchange interaction in occupied orbital energies is given by

$$\varepsilon_{i\sigma}^{\text{SI}}(E_x^{\text{Slater}}) = \left( i_{\sigma} \left| \frac{\delta E_x^{\text{Slater}}}{\delta \rho} [\rho_{i\sigma}] \right| i_{\sigma} \right) = \sum_{\sigma} -\frac{4}{3} C_X \rho_{i\sigma}^{4/3}. \quad (14.16)$$

The self-interaction of the Coulomb interaction in orbital energies is given by

$$\varepsilon_{i\sigma}^{\text{SI}}(E_{\text{Coulomb}}) = (i_{\sigma} i_{\sigma} | i_{\sigma} i_{\sigma}). \quad (14.17)$$

Suppose that the following relation is satisfied:

$$E_x^{\text{Slater}}[\rho_{i\sigma}] = - \int C_X \rho_{i\sigma}^{4/3} d\mathbf{r} \approx E_x^{\text{HF}}[\rho_{i\sigma}] = \frac{1}{2} (i_{\sigma} i_{\sigma} | i_{\sigma} i_{\sigma}). \quad (14.18)$$

The assumption is justified by the fact that the Slater-Dirac exchange functional can reproduce approximately 90 % of the HFx [3]. The condition for being SIF is

$$\varepsilon_{i\sigma}^{\text{SI}}(E_x^{\text{Slater}}) = \varepsilon_{i\sigma}^{\text{SI}}(E_{\text{Coulomb}}). \quad (14.19)$$

For the Slater-Dirac exchange, the next relation is instead obtained using Eq. (14.18):

$$\varepsilon_{i\sigma}^{\text{SI}}(E_x^{\text{Slater}}) = \frac{2}{3} \varepsilon_{i\sigma}^{\text{SI}}(E_{\text{Coulomb}}). \quad (14.20)$$

Therefore, the self-interaction of HFx is approximately underestimated by a factor of 2/3. The underestimation of HFx leads to larger SIEs in orbital energies than those in total energies.

### 14.2.4 Brief Summary

We applied the SIC- $\Delta$ SCF and SIC-TDDFT methods to CO core excitations. The SIC- $\Delta$ SCF and SIC-TDDFT methods are supposed to provide more accurate core-excitation energies than those of the  $\Delta$ SCF and TDDFT methods because of the absence of self-interaction. However, the SIC-TDDFT severely overestimates core-excitation energies, while the SIC- $\Delta$ SCF method slightly overestimates. These behaviors originate in the fact that the error cancellation occurs for the  $\Delta$ SCF method but does not occur for TDDFT. The present analysis suggests that the reduction of self-interaction is important for the TDDFT calculations. Based on the analysis, we have developed a new XC functional, CV-B3LYP with the appropriate inclusion of HFx, which reduces self-interaction [50–52].

## 14.3 Development of Core-Valence B3LYP for Second-Row Elements

The theoretical analysis [47] on core orbitals given in the previous section and numerical assessment [46] on widely used DFT functionals motivated us to develop CV-B3LYP, which is designed to select appropriate HFx portions for core and valence orbitals. First, the theory for CV-B3LYP is introduced, and its numerical assessment is subsequently demonstrated.

### 14.3.1 Theory for Core-Valence B3LYP Functional

#### 14.3.1.1 Energy Expression of Core-Valence B3LYP

The appropriate portion of HFx for core excitations is different from that for valence excitations [46]: BHHLYP including 50 % portions of HFx is appropriate for the descriptions of core excitations, while B3LYP with 20 % portions of HFx is well known to show better performance for valence excitations as well as other valence properties than BHHLYP. Therefore, the newly developed CV-B3LYP functional is designed to use appropriate portions of HFx for core and valence regions separately. In CV-B3LYP, the electronic energy is decomposed into core-core (cc), core-valence (cv), and valence-valence (vv) interactions, and the portions of HFx in the cc, cv, and vv interactions are determined, respectively. Thus, while the XC energy  $E_{xc}$  of B3LYP or BHHLYP is written by

$$E_{xc} = a \sum_{ij} (-K_{ij}) + bE_x^{\text{Slater}} + cE_x^{\text{B88}} + dE_c^{\text{VWN5}} + eE_c^{\text{LYP}}, \quad (14.21)$$

**Table 14.6** Coefficients of XC functionals in the BHHLYP, B3LYP, and CV-B3LYP functionals

	TDHF	BHHLYP	B3LYP	BLYP	CV-B3LYP		
					cc	cv	vv
$a$ (HFx)	1	0.5	0.2	0	0.5	0.35	0.2
$b$ (Slater-Dirac exchange)	0	0	0.08	0	0	0.04	0.08
$c$ (B88 exchange)	0	0.5	0.72	1	0.5	0.61	0.72
$d$ (VWN5 correlation)	0	0	0.19	0	0	0.095	0.81
$e$ (LYP correlation)	0	1	0.81	1	1	0.905	0.19

Coefficients in CV-B3LYP are given for each index

that of CV-B3LYP is given as

$$\begin{aligned}
E_{xc} = & a_{cc} \sum_{kl}^c (-K_{kl}) + a_{cv} \sum_k^c \sum_m^v (-K_{km}) + a_{cv} \sum_m^v \sum_k^c (-K_{mk}) + a_{vv} \sum_{mn}^v (-K_{mn}) \\
& + b_{cc} E_x^{\text{Slater}}[\rho_c] + b_{cv} (E_x^{\text{Slater}}[\rho] - E_x^{\text{Slater}}[\rho_c] - E_x^{\text{Slater}}[\rho_v]) + b_{vv} E_x^{\text{Slater}}[\rho_v] \\
& + c_{cc} E_x^{\text{B88}}[\rho_c] + c_{cv} (E_x^{\text{B88}}[\rho] - E_x^{\text{B88}}[\rho_c] - E_x^{\text{B88}}[\rho_v]) + c_{vv} E_x^{\text{B88}}[\rho_v] \\
& + d_{cc} E_c^{\text{VWN}}[\rho_c] + d_{cv} (E_c^{\text{VWN}}[\rho] - E_c^{\text{VWN}}[\rho_c] - E_c^{\text{VWN}}[\rho_v]) + d_{vv} E_c^{\text{VWN}}[\rho_v] \\
& + e_{cc} E_c^{\text{LYP}}[\rho_c] + e_{cv} (E_c^{\text{LYP}}[\rho] - E_c^{\text{LYP}}[\rho_c] - E_c^{\text{LYP}}[\rho_v]) + e_{vv} E_c^{\text{LYP}}[\rho_v].
\end{aligned} \tag{14.22}$$

where the  $a$ ,  $b$ ,  $c$ ,  $d$ , and  $e$  are the coefficients of HFx, Slater-Dirac exchange, B88 exchange, VWN5 correlation, and LYP correlation functionals, respectively. The subscripts  $i$  and  $j$  for occupied orbitals,  $a$  and  $b$  for virtual orbitals, and  $p$ ,  $q$ ,  $r$ , and  $s$  for general orbitals are used; occupied orbitals are classified into core orbitals  $k$  and  $l$ , and valence orbitals as  $m$  and  $n$ . The appropriate portions of HFx can be used by determining  $a_{cc}$ ,  $a_{cv}$ , and  $a_{vv}$  adequately. The practical values of the coefficients used in this study are shown in Table 14.6.  $\rho$ ,  $\rho_c$ , and  $\rho_v$  are the total, core, and valence electron densities:

$$\rho = \sum_i^{\text{occ}} |\phi_i|^2, \quad \rho_c = \sum_k^c |\phi_k|^2, \quad \rho_v = \sum_m^v |\phi_m|^2. \tag{14.23}$$

For the exchange and correlation functionals, the contributions of  $\rho_c$  and  $\rho_v$  correspond to the cc and vv interactions. Since cv elements of the density are zero, the cv interaction is represented as the subtraction of  $E_{xc}[\rho_c]$  and  $E_{xc}[\rho_v]$  from  $E_{xc}[\rho]$ .

### 14.3.1.2 Kohn-Sham Equation for Core-Valence B3LYP

In CV-B3LYP, electronic energy is decomposed into cc, cv, and vv interactions:

$$\begin{aligned}
 E = & 2 \sum_k^c H_k + 2 \sum_m^v H_m + \sum_{k>l}^c 2J_{kl} + \sum_k^c \sum_m^v 2J_{km} + \sum_m^v \sum_k^c 2J_{mk} + \sum_{m>n}^v 2J_{mn} \\
 & + a_{cc} \sum_{kl}^c (-K_{kl}) + a_{cv} \sum_k^c \sum_m^v (-K_{km}) + a_{cv} \sum_m^v \sum_k^c (-K_{mk}) + a_{vv} \sum_{mn}^v (-K_{mn}) \\
 & + b'_{cc} E_{xc}[\rho_c] + b'_{cv} (E_{xc}[\rho] - E_{xc}[\rho_c] - E_{xc}[\rho_v]) + b'_{vv} E_{xc}[\rho_v], \tag{14.24}
 \end{aligned}$$

where the exchange and correlation functionals  $E_x$  and  $E_c$  are collected as  $E_{xc}$  with the coefficient  $b'$ . The coefficients in the XC energies depend on the combinations of the orbitals. We define the Coulomb operators  $J_c$  and  $J_v$  associated with the core and valence orbitals, respectively, the total Coulomb operator  $J_{tot}$ , HFx operators  $K_c$  and  $K_v$ , and the first derivatives of  $E_{xc}[\rho]$ ,  $E_{xc}[\rho_c]$ , and  $E_{xc}[\rho_v]$  by

$$\begin{aligned}
 J_c &= \sum_k^c J_k, \quad J_v = \sum_m^v J_m, \quad J_{tot} = \sum_i^{occ} J_i = J_c + J_v, \\
 K_c &= \sum_k^c K_k, \quad K_v = \sum_m^v K_m, \\
 V_{xc}[\rho] &= \frac{\delta E_{xc}[\rho]}{\delta \rho}, \quad V_{xc}[\rho_c] = \frac{\delta E_{xc}[\rho_c]}{\delta \rho_c}, \quad V_{xc}[\rho_v] = \frac{\delta E_{xc}[\rho_v]}{\delta \rho_v}. \tag{14.25}
 \end{aligned}$$

By applying the variational principle to Eq. (14.4), two Fock operators are obtained:

$$F_c = h + 2J_{tot} - (a_{cc}K_c + a_{cv}K_v) + (b'_{cc} - b'_{cv})V_{xc}[\rho_c] + b'_{cv}V_{xc}[\rho], \tag{14.26}$$

$$F_v = h + 2J_{tot} - (a_{cv}K_c + a_{vv}K_v) + (b'_{vv} - b'_{cv})V_{xc}[\rho_v] + b'_{cv}V_{xc}[\rho]. \tag{14.27}$$

To combine these two Fock operators, we use the coupling-operator technique of Roothaan [72–74]. Since the invariance under the unitary transformation between core and valence orbitals is not guaranteed, Euler equations have the form

$$F_c \phi_k = \phi_k \varepsilon_{kk} + \sum_m^v \phi_m \theta_{mk}, \tag{14.28}$$

$$F_v \phi_m = \phi_m \varepsilon_{mm} + \sum_k^c \phi_k \theta_{km}. \tag{14.29}$$

To satisfy the Hermiticity of  $\epsilon$  matrix, the following condition should be imposed:

$$\epsilon_{km} = \langle \phi_k | F_c | \phi_m \rangle = \langle \phi_m | F_v | \phi_k \rangle = \epsilon_{mk}. \quad (14.30)$$

This condition leads to the coupling operators:

$$\left[ F_c - \sum_m^v |\phi_m\rangle \langle \phi_m| \Theta_c \right] |\phi_k\rangle = \sum_l^c |\phi_l\rangle \langle \phi_l| F_c |\phi_k\rangle, \quad (14.31)$$

$$\left[ F_v - \sum_k^c |\phi_k\rangle \langle \phi_k| \Theta_v \right] |\phi_m\rangle = \sum_n^v |\phi_n\rangle \langle \phi_n| F_v |\phi_m\rangle, \quad (14.32)$$

where  $\Theta_c$  and  $\Theta_v$  are defined as

$$\Theta_c = (1 - \lambda) F_c + \lambda F_v, \quad (14.33)$$

$$\Theta_v = \mu F_c + (1 - \mu) F_v. \quad (14.34)$$

Here,  $\lambda$  and  $\mu$  are arbitrary nonzero numbers. To ensure the Hermiticity of the left-hand sides of Eqs. (14.31) and (14.32), we define  $R_c$  and  $R_v$  as

$$R_c = - \sum_m^v \{ |\phi_m\rangle \langle \phi_m| \Theta_c \} + \{ \Theta_c | \phi_m\rangle \langle \phi_m| \}, \quad (14.35)$$

$$R_v = - \sum_k^c \{ |\phi_k\rangle \langle \phi_k| \Theta_v \} + \{ \Theta_v | \phi_k\rangle \langle \phi_k| \}, \quad (14.36)$$

and obtain the following equations:

$$(F_c + R_c) |\phi_k\rangle = \sum_l^c |\phi_l\rangle \theta_{lk} = |\phi_k\rangle \epsilon'_k, \quad (14.37)$$

$$(F_v + R_v) |\phi_m\rangle = \sum_n^v |\phi_n\rangle \theta_{nm} = |\phi_m\rangle \epsilon'_m. \quad (14.38)$$

The above-mentioned technique corresponds to the Roothaan double-Fock operator method. In the present study,  $\lambda$  and  $\mu$  are set to 0.5 and  $-0.5$ , which simplify the operators in the left-hand side of Eqs. (14.37) and (14.38) to  $0.5(F_c - F_v)$  for core-valence elements. In this case, the one-electron operator and Coulomb operator in  $F_c$  and  $F_v$  are canceled out and only exchange terms remain. The virtual-virtual elements of the Fock matrices are arbitrary when we use the double-Fock operator method. The present study adopted  $F_v$  as the virtual-virtual Fock matrix so that the virtual orbitals of CV-B3LYP are close to those of B3LYP.

### 14.3.2 Assessment of the Core-Valence B3LYP Functional

The CV-B3LYP functional was implemented into the GAMESS program [75]. When solving the KS equations, we determined the coefficients in Eq. (14.22) as listed in Table 14.6. The coefficients of cc and vv are set to those of BHHLYP and B3LYP, respectively. The coefficients of cv interactions are set to the mean values of those of BHHLYP and B3LYP. The standard enthalpies of formation for the G2-1 set were calculated by the procedure mentioned in Ref. [76] with the use of the cc-pVTZ basis sets of Dunning. In the subsequent TDDFT calculations, we approximately used the matrix form of B3LYP with CV-B3LYP orbital energies and orbital coefficients instead of implementing the TDDFT equations with CV-B3LYP, which are rigorously formulated above. It means that  $a_{cc}$ ,  $a_{cv}$ ,  $a_{vc}$ , and  $a_{vv}$  are equal to  $a$  of B3LYP, and  $b'_{cc}$ ,  $b'_{cv}$ ,  $b'_{vc}$ , and  $b'_{vv}$  are equal to  $b'$  of B3LYP. The basis sets used for the calculations of the excitation energies were the cc-pCVTZ basis set of Dunning. All molecular structures are optimized at B3LYP/6-31G(2df,p) [77] level for the calculation of standard enthalpies of formation and at B3LYP/cc-pVTZ level for those of excitation energies.

#### 14.3.2.1 Orbital Energies and Standard Enthalpies of Formation

DFT calculations for the ground state were performed with BHHLYP, CV-B3LYP, and B3LYP. The calculated orbital energies of  $N_2$  molecule are summarized in Table 14.7. The differences from experimental IPs with minus signs are shown in parentheses. For CV-B3LYP, KS equations proposed above were solved. In Table 14.7, two core- and four valence-occupied orbital energies are listed. The calculated core-orbital energies of CV-B3LYP are closer to those of BHHLYP than to those of B3LYP. The core-orbital energies of CV-B3LYP and BHHLYP are about 13 eV lower than those of B3LYP. In contrast, the valence-orbital energies of CV-B3LYP are closer to those of B3LYP than to those of BHHLYP. The valence-orbital energies of CV-B3LYP and B3LYP are 2–4 eV higher than those of BHHLYP. Thus, it is confirmed that the orbital energies of CV-B3LYP behave according to the design of the functional.

**Table 14.7** Orbital energies of the  $N_2$  molecule using BHHLYP, CV-B3LYP, and B3LYP functionals with cc-pCVTZ in eV

Orbital	BHHLYP		CV-B3LYP		B3LYP		Expt. -IP
1s $\sigma$	-405.70	(4.20)	-405.05	(4.85)	-392.31	(17.59)	-409.9 <sup>a</sup>
1s $\sigma^*$	-405.62	(4.28)	-404.98	(4.92)	-392.26	(17.64)	(-409.9)
2s $\sigma$	-34.58	(-)	-30.83	(-)	-30.75	(-)	
2s $\sigma^*$	-17.60	(1.15)	-15.11	(3.64)	-15.03	(3.72)	-18.75 <sup>b</sup>
2p $\pi^*$	-14.57	(2.36)	-12.75	(4.18)	-12.78	(4.15)	-16.93 <sup>b</sup>
2p $\sigma$	-14.11	(1.47)	-11.79	(3.79)	-11.78	(3.80)	-15.58 <sup>b</sup>

<sup>a</sup>Ref. [78]

<sup>b</sup>Ref. [62]

**Table 14.8** Statistical data of differences from experimental standard enthalpies of formation for the G2-1 set using BHHLYP, CV-B3LYP, and B3LYP functionals with cc-pVTZ in kcal/mol

	BHHLYP	CV-B3LYP	B3LYP
MAE <sup>a</sup>	12.4	4.2	2.9
RMS <sup>b</sup>	15.8	5.5	4.1
MAX. (+)	51.3	22.5	19.2
MAX. (−)	−7.5	−6.8	−7.8

<sup>a</sup>Mean absolute error

<sup>b</sup>Root mean square

All orbital energies are overestimated in comparison with experimental IPs with minus signs. For core orbitals, the deviations for B3LYP are more than 15 eV. BHHLYP reduces the deviations but still provides IPs with more than 4 eV deviations. For valence orbitals, the deviations are relatively smaller than those of core orbitals; BHHLYP estimates IPs within 2.5 eV.

The results for standard enthalpies of formation for the G2-1 set of 55 small molecules are shown in Table 14.8. The performance of CV-B3LYP is significantly better than that of BHHLYP and slightly worse than that of B3LYP: The mean absolute errors (MAEs) of CV-B3LYP, BHHLYP, and B3LYP are 4.2, 12.4, and 2.9 kcal/mol, respectively. The better performance of CV-B3LYP over BHHLYP is due to the improvement of the description of valence orbitals. The valence orbitals of CV-B3LYP are designed to be similar to those of B3LYP.

### 14.3.2.2 Excitation Energies

Table 14.9 shows the core- and valence-excitation energies of N<sub>2</sub> molecule calculated with the cc-pCVTZ basis set. The errors of the calculated results from the experimental values are shown in parentheses. The CT excitations are not numerically assessed here since CV-B3LYP determines the appropriate HFx portions for respective orbitals and does not have those optimized for well-separated occupied and unoccupied orbitals involved in the CT excitations. The 1s → 2pπ\* core-excitation energy of CV-B3LYP is close to that of BHHLYP: The errors of CV-B3LYP and BHHLYP are 0.3 and −3.0 eV, respectively. B3LYP yields the largest error, −12.5 eV. For the valence excitations, the accuracy of CV-B3LYP is comparable to that of B3LYP. BHHLYP fails to reproduce the order of the <sup>1</sup>Π<sub>g</sub>, <sup>1</sup>Π<sub>u</sub><sup>−</sup>, and <sup>1</sup>Δ<sub>u</sub> states because of the underestimation of the π → π\* excitation energies. CV-B3LYP represents the correct order of the three states as well as B3LYP does. The behavior of the excitation energies of CV-B3LYP in Table 14.9 corresponds to that of the orbital energies in Table 14.7, which significantly affect the calculated excitation energies.

Table 14.10 shows the 1s-π\* core-excitation energies of acetylene (C<sub>2</sub>H<sub>2</sub>), ethylene (C<sub>2</sub>H<sub>4</sub>), formaldehyde (CH<sub>2</sub>O), CO, and N<sub>2</sub> molecules. The deviations from the experimental values are shown in parentheses. The core-excitation energies of CV-B3LYP are close to those of BHHLYP rather than B3LYP for all molecules in

**Table 14.9** Excitation energies of the N<sub>2</sub> molecule using BHHLYP, CV-B3LYP, and B3LYP functionals with cc-pCVTZ (in eV)

	BHHLYP	CV-B3LYP	B3LYP	Expt.
1s → 2pπ*	398.0 (−3.0)	401.3 (+0.3)	388.5 (−12.5)	401.0 <sup>a</sup>
2pσ → 2pπ*( <sup>1</sup> Π <sub>g</sub> )	9.63 (+0.32)	9.47 (+0.16)	9.42 (+0.11)	9.31 <sup>b</sup>
2pπ → 2pπ*( <sup>1</sup> Σ <sub>u</sub> <sup>−</sup> )	9.05 (−0.87)	9.53 (−0.39)	9.52 (−0.40)	9.92 <sup>b</sup>
2pπ → 2pπ*( <sup>1</sup> Δ <sub>u</sub> )	9.59 (−0.68)	9.93 (−0.34)	9.92 (−0.35)	10.27 <sup>b</sup>

<sup>a</sup>Ref. [79]<sup>b</sup>Ref. [15]

Differences from the experimental data are shown in parentheses

**Table 14.10** 1s-π\*  
Core-excitation energies of  
C<sub>2</sub>H<sub>2</sub>, C<sub>2</sub>H<sub>4</sub>, CH<sub>2</sub>O, CO, and  
N<sub>2</sub> molecules using  
BHHLYP, CV-B3LYP, and  
B3LYP functionals (in eV)

Molecule	BHHLYP	CV-B3LYP	B3LYP	Expt.
<b>C<sub>2</sub>H<sub>2</sub></b>	283.6 (−2.2)	286.1 (+0.3)	275.3 (−10.5)	285.8 <sup>b</sup>
<b>C<sub>2</sub>H<sub>4</sub></b>	282.5 (−2.2)	285.1 (+0.4)	274.3 (−10.4)	284.7 <sup>b</sup>
<b>CH<sub>2</sub>O</b>	283.0 (−3.0)	286.0 (+0.0)	275.2 (−10.8)	286.0 <sup>b</sup>
<b>CO</b>	283.5 (−3.9)	286.9 (−0.5)	276.1 (−11.3)	287.4 <sup>b</sup>
<b>N<sub>2</sub></b>	397.9 (−3.1)	401.3 (+0.3)	388.5 (−12.5)	401.0 <sup>c</sup>
<b>CH<sub>2</sub>O</b>	528.1 (−2.7)	531.4 (+0.6)	516.7 (−14.1)	530.8 <sup>b</sup>
<b>CO</b>	531.6 (−2.6)	534.5 (+0.3)	519.8 (−14.4)	534.2 <sup>b</sup>
MAE <sup>a</sup>	2.8	0.3	12.0	

<sup>a</sup>Mean absolute error<sup>b</sup>Ref. [39]<sup>c</sup>Ref. [79]

Differences from the experimental data are shown in parentheses

Core excitations occur in bold atoms

Table 14.10. CV-B3LYP shows the best performance among the three functionals. The MAE of CV-B3LYP is about half of that of BHHLYP and considerably smaller than that of B3LYP: the MAEs of CV-B3LYP are less than 1 eV, while those of BHHLYP and B3LYP are more than 2 and 11 eV, respectively.

The valence-excitation energies of N<sub>2</sub>, C<sub>2</sub>H<sub>2</sub>, C<sub>2</sub>H<sub>4</sub>, *cis*-2-butene (*cis*-C<sub>4</sub>H<sub>8</sub>), 1,3-butadiene (C<sub>4</sub>H<sub>6</sub>), benzene (C<sub>6</sub>H<sub>6</sub>), 1,3,5-*trans*-hexatriene (C<sub>6</sub>H<sub>8</sub>), CH<sub>2</sub>O, and CO molecules are listed in Table 14.11. For valence excitations, the accuracy of CV-B3LYP is comparable to that of B3LYP: The MAEs of CV-B3LYP and B3LYP are 0.25 eV and that of BHHLYP is 0.36 eV. As is well known, the π → π\* excitation energy is red-shifted for longer π-conjugation systems. CV-B3LYP describes the red shift correctly as well as the conventional BHHLYP and B3LYP functionals.



**Table 14.11**  $\pi$ - $\pi^*$  valence-excitation energies of  $N_2$ ,  $C_2H_2$ ,  $C_2H_4$ ,  $C_4H_8$ ,  $C_4H_6$ ,  $C_6H_6$ ,  $C_6H_8$ ,  $CH_2O$ , and CO molecules using BHHLYP, CV-B3LYP, and B3LYP functionals in eV

Molecule	BHHLYP	CV-B3LYP	B3LYP	Expt.
$N_2$	9.05 (-0.87)	9.53 (-0.39)	9.52 (-0.40)	9.92 <sup>b</sup>
$C_2H_2$	6.62 (-0.48)	6.86 (-0.24)	6.86 (-0.24)	7.10 <sup>c</sup>
$C_2H_4$	7.87 (-0.13)	7.85 (-0.15)	7.90 (-0.10)	8.00 <sup>b</sup>
$C_4H_8$	7.18 (-0.37)	7.04 (-0.51)	7.04 (-0.51)	7.55 <sup>d</sup>
$C_4H_6$	6.04 (+0.12)	5.85 (-0.07)	5.85 (-0.07)	5.92 <sup>e</sup>
$C_6H_6$	5.69 (+0.79)	5.47 (+0.57)	5.46 (+0.56)	4.90 <sup>b</sup>
$C_6H_8$	5.01 (+0.06)	4.76 (-0.19)	4.76 (-0.19)	4.95 <sup>e</sup>
$CH_2O$	4.17 (+0.23)	4.06 (+0.12)	4.02 (+0.08)	3.94 <sup>b</sup>
CO	9.67 (-0.21)	9.82 (-0.06)	9.81 (-0.07)	9.88 <sup>b</sup>
MAE <sup>a</sup>	0.36	0.25	0.25	

<sup>a</sup>Mean absolute error

<sup>b</sup>Ref. [15]

<sup>c</sup>Ref. [80]

<sup>d</sup>Ref. [81]

<sup>e</sup>Ref. [82]

Differences from the experimental data are shown in parentheses

### 14.3.3 Brief Summary

We assessed the conventional XC functionals and proposed the new hybrid functional CV-B3LYP for the precise description of both core and valence excitations. By the assessment of TD-BLYP, TD-BHHLYP, TD-B3LYP, and TDHF methods, the portion of HFx is found to be important to describe core-excitation energies accurately. Based on this assessment, the CV-B3LYP functional is designed to possess the appropriate portions of HFx for core and valence regions separately. The KS equation for CV-B3LYP is derived using the coupling-operator method of Roothaan [72–74]. The TDDFT scheme for CV-B3LYP is also presented. DFT and TDDFT calculations are performed with the use of CV-B3LYP, BHHLYP, and B3LYP functionals. For the ground state, the orbital energies calculated with CV-B3LYP are close to those of BHHLYP and B3LYP for core and valence orbitals, respectively. CV-B3LYP reproduces standard enthalpies of formation for G2 set with reasonable accuracy as well as B3LYP does. TDDFT calculations demonstrate that the accuracy of CV-B3LYP is comparable to those of BHHLYP and B3LYP for core- and valence-excited states, respectively. The numerical results confirm that TDDFT calculations using CV-B3LYP are useful for describing both core- and valence-excited states with high accuracy.

## 14.4 Extension of Core-Valence B3LYP for Third-Row Elements

The core orbitals in the third-row elements have been also examined by estimating core-excitation energies [52]. The numerical assessment demonstrates that 70 and 50 % portions of HF $\alpha$  are appropriate for K-shell and L-shell electrons, which requires to modify CV-B3LYP so as to deal with three different HF $\alpha$  portions, 20, 50, and 70 % for valence, L-shell, and K-shell electrons. The following is the extension of CV-B3LYP.

### 14.4.1 Extension of Core-Valence B3LYP

In the previous CV-B3LYP [51, 52], the occupied orbitals are distinguished into core (C) and occupied-valence (OV) orbitals. In the present modified CV-B3LYP, the occupied orbitals are distinguished into three groups, namely, K-shell (C1), L-shell (C2), and occupied-valence (OV) orbitals. Thus, the electronic energy is decomposed into C1-C1, C1-C2, C1-OV, C2-C2, C2-OV, and OV-OV interactions:

$$\begin{aligned}
 E = & 2 \sum_k^{C1} H_k + 2 \sum_m^{C2} H_m + 2 \sum_p^{OV} H_p + \sum_{kl}^{C1} 2J_{kl} + \sum_k^{C1} \sum_m^{C2} 2J_{km} + \sum_k^{C1} \sum_p^{OV} 2J_{kp} \\
 & + \sum_m^{C2} \sum_k^{C1} 2J_{mk} + \sum_{mn}^{C2} 2J_{mn} + \sum_m^{C2} \sum_p^{OV} 2J_{mp} + \sum_p^{OV} \sum_k^{C1} 2J_{pk} + \sum_p^{OV} \sum_m^{C2} 2J_{pm} + \sum_{pq}^{OV} 2J_{pq} \\
 & + a_{C1C1} \sum_{kl}^{C1} (-K_{kl}) + a_{C1C2} \sum_k^{C1} \sum_m^{C2} (-K_{km}) + a_{C1OV} \sum_k^{C1} \sum_p^{OV} (-K_{kp}) \\
 & + a_{C2C2} \sum_m^{C2} \sum_k^{C1} (-K_{mk}) + a_{C2C2} \sum_{mn}^{C2} (-K_{mn}) + a_{C2OV} \sum_m^{C2} \sum_p^{OV} (-K_{mp}) \\
 & + a_{C1OV} \sum_p^{OV} \sum_k^{C1} (-K_{pk}) + a_{C2OV} \sum_p^{OV} \sum_m^{C2} (-K_{pm}) + a_{OV OV} \sum_{pq}^{OV} (-K_{pq}) \\
 & + b_{C1C1} E_{xc} [\rho_{C1}] + b_{C2C2} E_{xc} [\rho_{C2}] + b_{OV OV} E_{xc} [\rho_{OV}] \\
 & + b_{C1C2} (E_{xc} [\rho_{C1+C2}] - E_{xc} [\rho_{C1}] - E_{xc} [\rho_{C2}]) \\
 & + b_{C1OV} (E_{xc} [\rho_{C1+OV}] - E_{xc} [\rho_{C1}] - E_{xc} [\rho_{OV}]) \\
 & + b_{C2OV} (E_{xc} [\rho_{C2+OV}] - E_{xc} [\rho_{C2}] - E_{xc} [\rho_{OV}]), \tag{14.39}
 \end{aligned}$$

**Table 14.12** Coefficients of XC functionals in the modified CV-B3LYP functional

	C1C1	C1C2	C1OV	C2C2	C2OV	OVOV
$a$ (HFX)	0.7	0.6	0.45	0.5	0.35	0.2
$b$ (Slater-Dirac exchange)	0	0	0.04	0	0.04	0.08
(B88 exchange)	0.3	0.4	0.51	0.5	0.61	0.72
(VWN5 correlation)	0	0	0.095	0	0.095	0.19
(LYP correlation)	1	1	0.905	1	0.905	0.81

where  $H$  and  $J$  are one-electron and Coulomb integrals.  $a$  and  $b$  are the coefficients of HFX and DFT XC functionals. The “C1,” “C2,” and “OV” on the  $\Sigma$  mean that the summation runs over the K-shell, L-shell, and occupied-valence orbitals, respectively; therefore, suffixes  $(k, l)$ ,  $(m, n)$ , and  $(p, q)$  correspond to K-shell, L-shell, and occupied-valence orbitals. The definitions of the electron densities are as follows:

$$\rho_{C1} = \sum_k^{C1} |\phi_k|^2, \quad \rho_{C2} = \sum_m^{C2} |\phi_m|^2, \quad \rho_{OV} = \sum_p^{OV} |\phi_p|^2,$$

$$\rho_{C1+C2} = \sum_i^{\neq OV} |\phi_i|^2, \quad \rho_{C1+OV} = \sum_i^{\neq C2} |\phi_i|^2, \quad \rho_{C2+OV} = \sum_i^{\neq C1} |\phi_i|^2. \quad (14.40)$$

$\phi$  is the Kohn-Sham orbital. The “ $\neq C1$ ”, “ $\neq C2$ ”, and “ $\neq OV$ ” on the  $\Sigma$  mean that the summation runs over all occupied orbitals without the K-shell, L-shell, and occupied-valence orbitals, respectively. The C1-C2 interaction is represented as the subtraction of  $E_{xc}[\rho_{C1}]$  and  $E_{xc}[\rho_{C2}]$  from  $E_{xc}[\rho_{C1+C2}]$ , and the same applies to C1-OV and C2-OV interactions. In Eq. (14.39), the three- and higher-body interactions in DFT XC energies are neglected. However, our preliminary calculations have shown that the energy differences due to the truncation are small enough to be negligible. The XC functional in CV-B3LYP consists of Slater exchange, B88 exchange, VWN5 correlation, and LYP correlation functionals. The coefficients  $a_Y$  and  $b_Y$  ( $Y = C1C1, C1C2, C1OV, C2C2, C2OV,$  and  $OVOV$ ) used in the present calculations are listed in Table 14.12. The coefficients of C1C1, C2C2, and OVOV are set to those of HF + B88 + LYP (70%), BHHLYP, and B3LYP. The coefficients of C1C2, C1OV, and C2OV are set to the mean values of  $\{C1C1$  and  $C2C2\}$ ,  $\{C1C1$  and  $OVOV\}$ , and  $\{C2C2$  and  $OVOV\}$ , respectively. The sum of the coefficients in each group becomes 1.

Applying the variational principle to Eq. (14.39) leads to three kinds of Fock operators:

$$F_{C1} = h + 2J - (a_{C1C1}K_{C1} + a_{C1C2}K_{C2} + a_{C1OV}K_{OV})$$

$$+ (b_{C1C1} - b_{C1C2} - b_{C1OV})V_{xc}[\rho_{C1}] + b_{C1C2}V_{xc}[\rho_{C1+C2}] + b_{C1OV}V_{xc}[\rho_{C1+OV}], \quad (14.41)$$

$$\begin{aligned}
F_{C2} = & h + 2J - (a_{C1C2}K_{C1} + a_{C2C2}K_{C2} + a_{C2OV}K_{OV}) \\
& + (b_{C2C2} - b_{C1C2} - b_{C2OV}) V_{xc} [\rho_{C2}] + b_{C1C2} V_{xc} [\rho_{C1+C2}] + b_{C2OV} V_{xc} [\rho_{C2+OV}],
\end{aligned} \tag{14.42}$$

$$\begin{aligned}
F_{OV} = & h + 2J - (a_{C1OV}K_{C1} + a_{C2OV}K_{C2} + a_{OV OV}K_{OV}) \\
& + (b_{OV OV} - b_{C1OV} - b_{C2OV}) V_{xc} [\rho_{OV}] + b_{C1OV} V_{xc} [\rho_{C1+OV}] + b_{C2OV} V_{xc} [\rho_{C2+OV}].
\end{aligned} \tag{14.43}$$

$h$  is one-electron operator.  $J$  and  $K$  in and after Eq. (14.41) are Coulomb and HFX operators. HFX operators and the first derivatives of  $E_{xc}$  are as follows:

$$\begin{aligned}
K_{C1} &= \sum_k^{C1} K_k, \quad K_{C2} = \sum_m^{C2} K_m, \quad K_{OV} = \sum_p^{OV} K_p, \\
V_{xc} [\rho_{C1}] &= \frac{\delta E_{xc} [\rho_{C1}]}{\delta \rho_{C1}}, \quad V_{xc} [\rho_{C2}] = \frac{\delta E_{xc} [\rho_{C2}]}{\delta \rho_{C2}}, \quad V_{xc} [\rho_{OV}] = \frac{\delta E_{xc} [\rho_{OV}]}{\delta \rho_{OV}}, \\
V_{xc} [\rho_{C1+C2}] &= \frac{\delta E_{xc} [\rho_{C1+C2}]}{\delta \rho_{C1+C2}}, \quad V_{xc} [\rho_{C1+OV}] = \frac{\delta E_{xc} [\rho_{C1+OV}]}{\delta \rho_{C1+OV}}, \\
V_{xc} [\rho_{C2+OV}] &= \frac{\delta E_{xc} [\rho_{C2+OV}]}{\delta \rho_{C2+OV}}.
\end{aligned} \tag{14.44}$$

In order to guarantee the invariance under the unitary transformation, the coupling-operator technique of Roothaan is adopted. Introducing the operators  $R$ ,

$$\begin{aligned}
R_{C1} = & - \sum_m^{C2} \{ |\phi_m\rangle \langle \phi_m| \Theta_{C1C2} \} + (\Theta_{C1C2} |\phi_m\rangle \langle \phi_m|) \\
& - \sum_p^{OV} \{ |\phi_p\rangle \langle \phi_p| \Theta_{C1OV} \} + (\Theta_{C1OV} |\phi_p\rangle \langle \phi_p|),
\end{aligned} \tag{14.45}$$

$$\begin{aligned}
R_{C2} = & - \sum_k^{C1} \{ |\phi_k\rangle \langle \phi_k| \Theta_{C2C1} \} + (\Theta_{C2C1} |\phi_k\rangle \langle \phi_k|) \\
& - \sum_p^{OV} \{ |\phi_p\rangle \langle \phi_p| \Theta_{C2OV} \} + (\Theta_{C2OV} |\phi_p\rangle \langle \phi_p|),
\end{aligned} \tag{14.46}$$

$$\begin{aligned}
R_{OV} = & - \sum_k^{C1} \{ |\phi_k\rangle \langle \phi_k| \Theta_{OV C1} \} + (\Theta_{OV C1} |\phi_k\rangle \langle \phi_k|) \\
& - \sum_m^{C2} \{ |\phi_m\rangle \langle \phi_m| \Theta_{OV C2} \} + (\Theta_{OV C2} |\phi_m\rangle \langle \phi_m|),
\end{aligned} \tag{14.47}$$

we obtain the following:

$$F'_{C1} = F_{C1} + R_{C1}, \quad (14.48)$$

$$F'_{C2} = F_{C2} + R_{C2}, \quad (14.49)$$

$$F'_{OV} = F_{OV} + R_{OV}, \quad (14.50)$$

where  $\Theta$ s are

$$\Theta_{C1C2} = (1 - \lambda) F_{C1} + \lambda F_{C2}, \quad (14.51)$$

$$\Theta_{C2C1} = -\lambda F_{C1} + (1 + \lambda) F_{C2}, \quad (14.52)$$

$$\Theta_{C1OV} = (1 - \mu) F_{C1} + \mu F_{OV}, \quad (14.53)$$

$$\Theta_{OVC1} = -\mu F_{C1} + (1 + \mu) F_{OV}, \quad (14.54)$$

$$\Theta_{C2OV} = (1 - \sigma) F_{C2} + \sigma F_{OV}, \quad (14.55)$$

$$\Theta_{OVC2} = -\sigma F_{C2} + (1 + \sigma) F_{OV}. \quad (14.56)$$

$\lambda$ ,  $\mu$ , and  $\sigma$  are arbitrary nonzero numbers and set to 0.1 in the present study. Thus, Fock operator for occupied orbitals is rewritten as follows:

$$F = \sum_k^{C1} F'_{C1} |\phi_k\rangle \langle \phi_k| + \sum_m^{C2} F'_{C2} |\phi_m\rangle \langle \phi_m| + \sum_p^{OV} F'_{OV} |\phi_p\rangle \langle \phi_p|. \quad (14.57)$$

The virtual orbitals are treated in the similar way as the previous CVR-B3LYP [51], in which Rydberg orbitals are distinguished by using second moments of the orbitals.  $F_{OV}$  and the Fock operators formed in HF method were adopted as the Fock operator forms of unoccupied-valence and Rydberg orbitals, respectively. In the TDDFT calculations, we adopted an approximation similar to that for previous studies [50–52], in which we used the **A** and **B** matrix forms of B3LYP, while using the orbital energies and coefficients of CVR-B3LYP.

#### 14.4.2 Assessment of Modified Core-Valence B3LYP

The descriptions of K-shell, L-shell, and valence electrons by the modified CV-B3LYP functional are assessed by calculating core- and valence-excitation energies

**Table 14.13** 1s and 2p core-excitation energies of SiH<sub>4</sub>, PH<sub>3</sub>, H<sub>2</sub>S, HCl, and Cl<sub>2</sub> molecules by TDDFT with the modified CV-B3LYP functional with cc-pCVTZ plus Rydberg basis functions in eV

Molecule	1s excitation			2p excitation		
	Assignment	CV-B3LYP	Expt.	Assignment	CV-B3LYP	Expt.
SiH <sub>4</sub>	Si1s → σ*	1846.6 (+4.1)	1842.5 <sup>b</sup>	Si2p → σ*	103.7 (+0.9)	102.8 <sup>f,g</sup>
PH <sub>3</sub>	P1s → σ*(e)	2148.9 (+3.1)	2145.8 <sup>c</sup>	P2p → σ*	133.1 (+0.8)	132.3 <sup>f,g</sup>
H <sub>2</sub> S	S1s → 3b <sub>2</sub> (σ*)	2474.7 (+1.6)	2473.1 <sup>d</sup>	S2p → σ*	166.1 (+1.6)	164.5 <sup>h</sup>
	S1s → 4pb <sub>2</sub>	2477.4 (+1.1)	2476.3 <sup>d</sup>	S2p → 4s	168.3 (+1.8)	166.5 <sup>h</sup>
HCl	Cl1s → 3pσ*	2824.8 (+0.9)	2823.9 <sup>c</sup>	Cl2pπ → 3pσ*	202.0 (+1.0)	201.0 <sup>f</sup>
	Cl1s → 4pπ	2827.9 (+0.1)	2827.8 <sup>c</sup>	Cl2pπ → 4pπ	205.0 (+0.4)	204.6 <sup>f</sup>
Cl <sub>2</sub>	Cl1s → 3pσ <sub>u</sub> *	2822.1 (+0.8)	2821.3 <sup>c</sup>	Cl2pπ → 3pσ <sub>u</sub> *	199.1 (+0.4)	198.7 <sup>g,i</sup>
	Cl1s → 4p	2829.2 (+0.7)	2828.5 <sup>c</sup>	Cl2pπ → 4s	205.8 (+1.0)	204.8 <sup>g,i</sup>
MAE <sup>a</sup>		1.5			1.0	

<sup>a</sup>Mean absolute error<sup>b</sup>Ref. [84]<sup>c</sup>Ref. [85]<sup>d</sup>Ref. [86]<sup>e</sup>Ref. [87]<sup>f</sup>Ref. [88]<sup>g</sup>Ref. [89]<sup>h</sup>Ref. [90]<sup>i</sup>Ref. [91]

and standard enthalpies of formations. In the CV-B3LYP calculations, the portions of HFx for K-shell, L-shell, and occupied-valence orbitals were determined to 70, 50, and 20 % by using the coefficients given in Table 14.12. The scalar relativistic effects were included by using the relativistic scheme by eliminating small-components (RESC) method [83]. The basis sets and geometries of molecules used in CV-B3LYP calculations are the same as those used in Sect. 14.3 [52].

Table 14.13 shows the 1s and 2p core-excitation energies of SiH<sub>4</sub>, PH<sub>3</sub>, H<sub>2</sub>S, HCl, and Cl<sub>2</sub> molecules calculated with the modified CV-B3LYP functional. The MAEs of CV-B3LYP in Table 14.13 (1.5, 1.1 eV) for (1s, 2p) core-excitation energies clarify that the modified CV-B3LYP provides well-balanced results for third-row elements. Thus, it is demonstrated that the modified CV-B3LYP shows high performance both for K-shell and L-shell core excitations.

In order to assess the accuracy of the description of occupied-valence electrons, excitation energies from occupied-valence orbitals of SiH<sub>4</sub>, PH<sub>3</sub>, H<sub>2</sub>S, HCl, and

**Table 14.14** Valence- and Rydberg-excitation energies of SiH<sub>4</sub>, PH<sub>3</sub>, H<sub>2</sub>S, HCl, and Cl<sub>2</sub> molecules by TDHF and TDDFT with BLYP, B3LYP, BHHLYP, and the modified CV-B3LYP functionals with cc-pCVTZ plus Rydberg basis functions (in eV)

Molecule	Assignment	BLYP	B3LYP	BHHLYP	TDHF	CV-B3LYP	Expt.
SiH <sub>4</sub>	t <sub>2</sub> → 4s	8.0	8.5	9.2	9.9	9.4	8.8 <sup>b</sup>
		(−0.8)	(−0.3)	(+0.4)	(+1.1)	(+0.6)	
PH <sub>3</sub>	n → 4p	6.8	7.2	8.0	8.4	8.8	7.8 <sup>c</sup>
		(−1.0)	(−0.6)	(+0.2)	(+0.6)	(+1.0)	
H <sub>2</sub> S	2b <sub>1</sub> → σ* <sub>g</sub>	5.8	6.0	6.1	6.2	6.0	5.5 <sup>c</sup>
		(+0.4)	(+0.5)	(+0.6)	(+0.8)	(+0.6)	
HCl	3pπ → 4s	8.3	8.9	9.8	10.5	9.8	9.6 <sup>d</sup>
		(−1.3)	(−0.7)	(+0.2)	(+0.9)	(+0.2)	
Cl <sub>2</sub>	π <sub>g</sub> → σ <sub>u</sub>	3.2	3.3	3.6	4.0	3.3	3.8 <sup>d</sup>
		(−0.6)	(−0.4)	(−0.2)	(+0.2)	(−0.5)	
MAE <sup>a</sup>		0.8	0.5	0.3	0.7	0.6	

<sup>a</sup>Mean absolute error<sup>b</sup>Ref. [92]<sup>c</sup>Ref. [93]<sup>d</sup>Ref. [94]

Cl<sub>2</sub> molecules were calculated by TDHF and TDDFT with B3LYP, BHHLYP, and the modified CV-B3LYP. Table 14.14 lists the calculated excited energies. In Table 14.14, BHHLYP shows high performance, and the accuracy of BLYP, B3LYP, and TDHF is slightly worse than BHHLYP: MAEs of BLYP, B3LYP, BHHLYP, and TDHF are 0.8, 0.5, 0.3, and 0.7 eV, respectively. The excitation energies of CV-B3LYP are close to and higher than those of B3LYP for occupied-valence → unoccupied-valence and occupied-valence → Rydberg excitations, respectively. This is because the valence and Rydberg orbitals of CV-B3LYP are designed to be similar to those of B3LYP and HF. The MAE of CV-B3LYP is 0.6 eV, which is comparable to that of B3LYP. Therefore, CV-B3LYP describes valence-excitation energies with reasonable accuracy as like as conventional DFT methods.

The standard enthalpies of formation of SiH<sub>4</sub>, PH<sub>3</sub>, H<sub>2</sub>S, HCl, and Cl<sub>2</sub> molecules, which are the valence-electron properties in the ground states, were calculated by the procedure mentioned in Ref. [76]. The results of HF and DFT calculations with the BLYP, B3LYP, BHHLYP, and CV-B3LYP functionals are shown in Table 14.15. DFT gives more accurate results than HF does: The MAE of HF method is 52.0 kcal/mol, while all of the MAEs of DFT are less than 10 kcal/mol. The accuracy of BLYP and B3LYP is significantly high among the DFT methods, whose MAEs are 2.0 and 1.5 kcal/mol. The accuracy of CV-B3LYP with the MAE of 1.9 kcal/mol is comparable to BLYP and B3LYP. Thus, we confirm that CV-B3LYP is capable of describing the behaviors of not only K-shell and L-shell electrons but also valence ones with reasonable accuracy, while BHHLYP is appropriate only for K-shell and L-shell excitations, respectively.

**Table 14.15** Standard enthalpies of formation of SiH<sub>4</sub>, PH<sub>3</sub>, H<sub>2</sub>S, SO<sub>2</sub>, HCl, and Cl<sub>2</sub> molecules by HF and DFT with the BLYP, B3LYP, BHHLYP, HF, and modified CV-B3LYP functionals with cc-pCVTZ plus Rydberg basis functions in eV

	BLYP	B3LYP	BHHLYP	HF	CV-B3LYP	Expt. <sup>b</sup>
SiH <sub>4</sub>	13.3 (+5.1)	7.9 (−0.3)	7.9 (−0.3)	75 (+66.8)	5.9 (−2.3)	8.2
PH <sub>3</sub>	1.2 (−0.1)	−0.4 (−1.7)	3.4 (+2.1)	71.7 (+70.4)	−2.5 (−3.8)	1.3
H <sub>2</sub> S	−2.8 (+2.1)	−3.7 (+1.2)	0.5 (+5.4)	48.7 (+53.6)	−5.4 (−0.5)	−4.9
HCl	−19.9 (+2.2)	−20.3 (+1.8)	−17.5 (+4.6)	7.7 (+29.8)	−21.5 (+0.6)	−22.1
Cl <sub>2</sub>	−0.5 (−0.5)	2.7 (+2.7)	10.3 (+10.3)	39.4 (+39.4)	2.1 (+2.1)	0.0
MAE <sup>a</sup>	2.0	1.5	4.5	52	1.9	

<sup>a</sup>Mean absolute error

<sup>b</sup>Ref. [76]

### 14.4.3 Brief Summary

The CV-B3LYP functional has been extended to core-excited-state calculations of the molecules containing third-row elements. Since the assessment of TDDFT calculations with conventional XC functionals demonstrates that 70 and 50 % portions of HFx are appropriate for calculating K-shell and L-shell core-excitation energies [52], the CV-B3LYP functional is modified to possess the appropriate portions of HFx for K-shell, L-shell, and occupied-valence regions separately. TDDFT calculations on several molecules containing third-row elements show that the modified CV-B3LYP functional reproduces the K-shell and L-shell core-excitation energies with reasonable accuracy. For valence properties, the calculations of valence-excitation energies and standard enthalpies of formation confirm that CV-B3LYP describes valence electrons accurately as well as B3LYP does. The numerical assessments have revealed the high accuracy of CV-B3LYP for the descriptions of all of the K-shell, L-shell, and valence electrons.

## 14.5 Development of Orbital-Specific Functionals

As explained in the previous sections, we have developed an OS hybrid functional: CV-B3LYP hybrid functional for second- and third-row elements [50–52]. However, the HFx portions were determined by the numerical assessments. A more physically motivated determination is demanded. To this end, we have used the linearity condition for orbital energies (LCOE) in order to construct XC functionals [53–56]. The LCOE is that the second derivative of the total energy with respect to occupation



numbers should be 0 [60, 94–98]. The LCOE has been investigated extensively: Yang group [95–97] discussed the LCOE for the highest occupied molecular orbital (HOMO). Vydrov et al. [98] and Song et al. [60] also examined the effect of the short- and long-range parts of HFx on the linearity, respectively. Livshits and Baer have used the LCOE for tuning a range-determining parameter [99]. Studies on the orbital energies related to Koopmans' theorem have been carried out by Salzner and Baer [100] and Tsuneda et al. [101].

This section explains how to use the LCOE to global hybrid functionals and assesses their performance regarding orbital energies. Numerical assessments on ionization potentials (IPs) and concluding remarks are also given.

## 14.5.1 Theory of Orbital-Specific Functionals

### 14.5.1.1 Linearity Condition for Orbital Energies

Janak's theorem [102] in KS-DFT states that the first derivative of the total energy with respect to the occupation number  $f_i$  of the  $i$ th KS orbital is equivalent to its orbital energy:

$$\frac{\partial E}{\partial f_i} = \varepsilon_i. \quad (14.58)$$

In particular, the following relation for HOMO is clarified by Almbladh and von Barth [103]:

$$\frac{\partial E}{\partial f_{\text{HOMO}}} = \varepsilon_{\text{HOMO}} = -\text{IP}. \quad (14.59)$$

Namely, the HOMO energy is proven to be equivalent to the first IP with the opposite sign. Since the IP should be constant, the following LCOE is derived:

$$\left. \frac{\partial E}{\partial f_i} \right|_{0 \leq f_i \leq 1} = \varepsilon_i = \text{const.}, \quad (14.60)$$

or

$$\left. \frac{\partial^2 E}{\partial f_i^2} \right|_{0 \leq f_i \leq 1} = \left. \frac{\partial \varepsilon_i}{\partial f_i} \right|_{0 \leq f_i \leq 1} = 0. \quad (14.61)$$

Although Eq. (14.61) is exact for HOMO, it may not be necessarily satisfied for the other orbitals. However, Eq. (14.61) can offer a better description since it can remove SIEs [47, 50–52].

### 14.5.1.2 Construction of Orbital-Specific Functionals

We describe two procedures of how to construct the OS global hybrid functionals using Eq. (14.61): the determination of OS parameters and estimation of orbital energies.

Assume that the XC functional has the following form:

$$E_{xc}[\alpha] = (1 - \alpha) E_x^{\text{DFT}} + \alpha E_x^{\text{HF}} + E_c^{\text{DFT}}, \quad (14.62)$$

where  $E_x^{\text{DFT}}$ ,  $E_x^{\text{HF}}$ , and  $E_c^{\text{DFT}}$  are the DFT exchange (DFTx), HFx, and DFT correlation (DFTc) energies, respectively.  $\alpha$  represents a portion for HFx. The corresponding orbital energy  $\varepsilon_{xc}[\alpha]$  is expressed as

$$\begin{aligned} \varepsilon_i[\alpha] &= \varepsilon_T + \varepsilon_{\text{Ne}} + \varepsilon_J + (1 - \alpha) \varepsilon_x^{\text{DFT}} + \alpha \varepsilon_x^{\text{HF}} + \varepsilon_c^{\text{DFT}} \\ &= (1 - \alpha) \{ \varepsilon_T + \varepsilon_{\text{Ne}} + \varepsilon_J + \varepsilon_x^{\text{DFT}} + \varepsilon_c^{\text{DFT}} \} + \alpha \{ \varepsilon_T + \varepsilon_{\text{Ne}} + \varepsilon_J + \varepsilon_x^{\text{HF}} + \varepsilon_c^{\text{DFT}} \}, \end{aligned} \quad (14.63)$$

where  $\varepsilon_T$ ,  $\varepsilon_{\text{Ne}}$ ,  $\varepsilon_J$ ,  $\varepsilon_x^{\text{DFT}}$ ,  $\varepsilon_x^{\text{HF}}$ , and  $\varepsilon_c^{\text{DFT}}$  are the kinetic, nuclear attraction, Coulomb, DFTx, HFx, and DFTc contributions for the orbital energy, respectively. Here, we introduce the assumption:

$$\varepsilon_i[\alpha] \cong (1 - \alpha) \varepsilon_i^{\text{DFT}} + \alpha \varepsilon_i^{\text{HF+DFTc}}. \quad (14.64)$$

$\varepsilon_i^{\text{DFT}}$  and  $\varepsilon_i^{\text{HF+DFTc}}$  represent the pure DFT and HF + DFTc orbital energies. As our previous assessment revealed [50–52], the OS  $\alpha$  exhibits an orbital dependence; therefore,  $\alpha_i$  for the  $i$ th KS orbital is determined as follows:

$$\left. \frac{\partial \varepsilon_i[\alpha_i]}{\partial f_i} \right|_{0 \leq f_i \leq 1} \cong (1 - \alpha_i) \left. \frac{\partial \varepsilon_i^{\text{DFT}}}{\partial f_i} \right|_{0 \leq f_i \leq 1} + \alpha_i \left. \frac{\partial \varepsilon_i^{\text{HF+DFTc}}}{\partial f_i} \right|_{0 \leq f_i \leq 1} = 0. \quad (14.65)$$

Then, the orbital energy is estimated with the determined  $\alpha_i$  by the following relation:

$$\varepsilon_i[\alpha_i] \cong (1 - \alpha_i) \varepsilon_i^{\text{DFT}} + \alpha_i \varepsilon_i^{\text{HF+DFTc}}. \quad (14.66)$$

Here, we choose the following DFT XC functionals: SVWN5, BLYP, Perdew-Burke-Ernzerhof (PBE) [9], Tao-Perdew-Staroverov-Scuseria (TPSS) [10] XC functionals.

The procedure of the estimation of the orbital energies is as follows: The derivatives  $\partial \varepsilon_i^{\text{DFT}} / \partial f_i$  and  $\partial \varepsilon_i^{\text{HF+DFTc}} / \partial f_i$  are numerically estimated at  $f_i = 1.0$  with  $\Delta f_i = 0.0001$ . Using the derivatives, we determine  $\alpha_i$  by Eq. (14.65) and estimate orbital energies by Eq. (14.66) using DFT and HF + DFTc orbital energies at  $f_i = 1.0$ . Namely, the OS global hybrid functionals are constructed for respective orbitals. All calculations are carried out by the modified version of the GAMESS program.

## 14.5.2 Numerical Applications

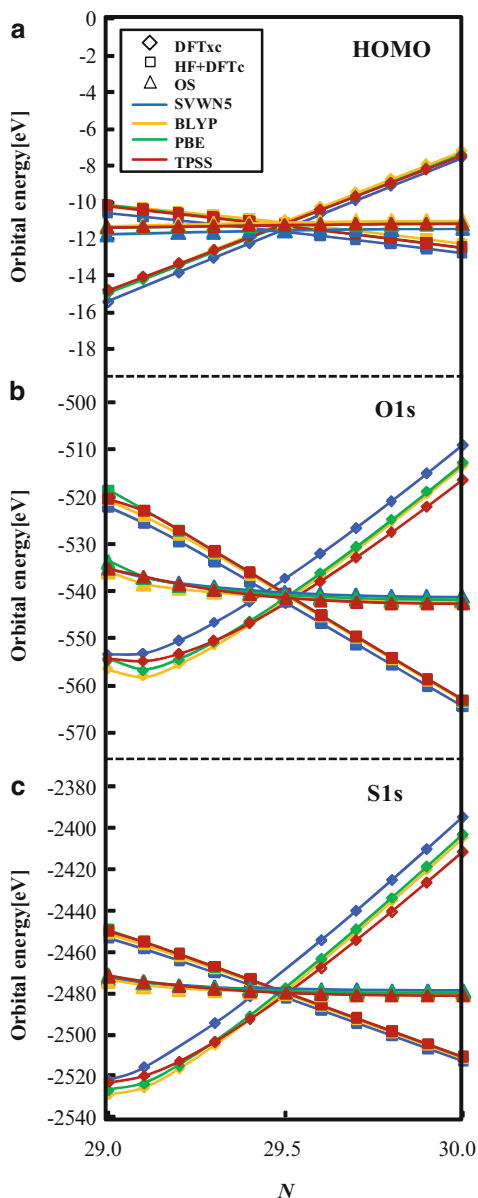
### 14.5.2.1 Orbital Energy for Fractional Occupation Numbers

The behavior of the orbital energies of OCS molecule is examined with respect to fractional occupation number (FON) electrons for the OS global hybrid functionals of SVWN5, BLYP, PBE, and TPSS XC functionals. The cc-pCVTZ basis set was adopted, and geometrical parameters were optimized at the B3LYP/cc-pVTZ level. Figures 14.1 demonstrate orbital energies of HOMO, O1s, and S1s of OCS molecule with respect to FON electrons. As shown in Fig. 14.1, HOMO energies decrease for HFX + DFTc functional as the number of electrons increases. This behavior is different from that of long-range corrected HFX + LYP [53]. Thus, the inclusion of short-range HFX varies the slopes of the HOMO energies. Contrarily, as the number of electrons increases, HOMO energies increase for the conventional DFT XC functionals, which is ascribed to SIE. The dependences of DFTc functionals for HFX + DFTc are slightly larger than those for the conventional XC functionals. The selection of appropriate  $\alpha_{\text{HOMO}}$  by the LCOE reproduces approximately constant curves for the OS global hybrid functional of the LDA, GGA, and meta-GGA functionals whose  $\alpha_{\text{HOMO}}$  are estimated to be approximately 0.75.

Figures 14.1 illustrate the O1s and S1s orbital energies with respect to FON electrons. A similar tendency is observed for the O1s and S1s orbitals: As the number of electrons increases, orbital energies of HFX + DFTc functional decrease and those of the conventional DFT XC functionals increase. In contrast to HOMO, the dependences of DFTc functionals for HFX + DFTc are smaller than those for the conventional XC functionals. The curves of the OS global hybrid functionals with appropriate  $\alpha_i$  determined through the LCOE are approximately flat for O1s and S1s. The OS parameters  $\{\alpha_{\text{O1s}}, \alpha_{\text{S1s}}\}$  are approximately  $\{0.57, 0.71\}$ , which are slightly larger than those of CV-B3LYP, determined by numerical assessment for core excitations [50–52].

In order to assess the performance of the OS global hybrid functionals from a different point of view, we also compare the orbital energies and IPs of valence and core orbitals for OCS molecule in a sense of Koopmans' theorem. IPs obtained by the OS hybrid functionals are shown in Table 14.16. The deviations from experimental IPs [53] and values of  $\alpha_i$  are shown in parentheses and square brackets, respectively. For HOMO, the OS global hybrid functionals provide comparatively similar IPs: 11.45, 10.99, 11.18, and 11.17 eV for SVWN5, BLYP, PBE, and TPSS functionals, and the corresponding deviations are at most 0.25 eV. The OS hybrid functionals also reproduce O1s and S1s IPs within the deviation of 2.5 eV for the LDA, GGA, and meta-GGA functionals, though the accurate estimation of large IPs is rather difficult.

**Fig. 14.1** Orbital energy variations  $\varepsilon_i$  [eV] of (a) HOMO, (b) O1s orbital, (c) S1s orbital of OCS as a function of the electron number  $N$



#### 14.5.2.2 IP and HFx Portion

For comparative assessment, IPs were estimated for eight molecules containing not only second- but also third-row elements: CO, H<sub>2</sub>O, NH<sub>3</sub>, HCHO, PH<sub>3</sub>, H<sub>2</sub>S, HCl, and OCS. The following XC functionals such as SVWN5, BLYP, PBE, and TPSS

**Table 14.16** OCS IPs (eV) by OS global hybrid functionals of SVWN5, BLYP, PBE, and TPSS functionals and  $\alpha_i$  determined for the OS in eV

	SVWN5		BLYP		PBE		TPSS		Expt. <sup>a</sup>
S1s	2478.81	(−1.49)	2480.68	(0.38)	2479.76	(−0.54)	2481.01	(0.71)	2480.3
	[0.7133]		[0.7125]		[0.7124]		[0.7011]		
O1s	541.1	(0.80)	542.29	(1.99)	541.94	(1.64)	542.64	(2.34)	540.3
	[0.5796]		[0.5777]		[0.5792]		[0.5623]		
HOMO	11.45	(0.25)	10.99	(−0.21)	11.18	(−0.02)	11.17	(−0.03)	11.2
	[0.7500]		[0.7496]		[0.7470]		[0.7426]		

<sup>a</sup>Ref. [53]**Table 14.17** Mean absolute errors of IPs estimated by conventional and OS global hybrid functionals of SVWN5, BLYP, PBE, and TPSS functionals in eV

Type	Functional	MAD			
		1s (P, S, Cl)	1s (C, N, O), 2s (S)	Valence	Overall
SVWN5	SVWN5	85.22	29.18	5.22	27.54
	OS SVWN5	0.60	1.41	0.48	0.85
	$[\alpha_i]$	[0.716]	[0.624]	[0.701]	[0.674]
BLYP	BLYP	74.88	25.58	5.42	24.56
	B3LYP	50.77	21.25	3.60	16.50
	OS BLYP	1.58	2.05	0.44	1.23
	$[\alpha_i]$	[0.715]	[0.621]	[0.698]	[0.671]
PBE	PBE	76.37	26.14	5.29	24.95
	PBE0	46.45	19.02	3.27	14.95
	OS PBE	0.88	1.70	0.44	0.98
	$[\alpha_i]$	[0.715]	[0.622]	[0.700]	[0.673]
TPSS	TPSS	67.93	23.07	5.05	22.29
	TPSSh	54.79	23.73	4.18	18.19
	OS TPSS	1.86	2.11	0.47	1.32
	$[\alpha_i]$	[0.704]	[0.608]	[0.693]	[0.663]

are examined for the OS global hybrid functionals. For comparison, the results of the OS functional of the LC hybrid functional, long-range corrected BLYP (LC-BLYP) [16], and the conventional XC functionals including pure and hybrid functionals are also tabulated. The geometries optimized at the B3LYP/cc-pVTZ level are adopted. For molecules containing third-row elements, the scalar relativistic effect is included by using the RESC method [82]. Table 14.17 lists MAEs from experimental IPs for conventional and OS XC functionals of LC-BLYP, SVWN5, BLYP, PBE, and TPSS using the cc-pCVTZ basis set. The mean values of  $\alpha_i$  are also shown in square brackets. The groups of {P1s, S1s, Cl1s} and {C1s, N1s, O1s, S2s} are labeled as C1 and C2 orbitals.

The conventional SVWN5 functional, which is a typical LDA functional, provides large MAEs owing to severe underestimation by SIEs [47], for example, 85.22 eV for 1s IPs of the third-row elements. The MAEs decrease from a deeper core to valence orbitals: 29.18 and 5.22 eV of C2 and valence orbitals, respectively.

On the other hand, the LCOE drastically reduces the MAEs: the overall MAE is 0.85 eV reduced from 27.54 eV, and the largest MAE is at most 1.41 eV for C2. The average determined  $\alpha_i$  values range 0.624–0.716.

The conventional BLYP and PBE functionals, which are typical GGA functionals, provide smaller MAEs than those of SVWN5 for core and inner valence orbitals. The tendency is similar to that of SVWN5: the larger IPs lead to larger deviations. A slight difference in the performance for HOMO is confirmed in comparison to SVWN5. The conventional hybrid functionals B3LYP and PBE-1-parameter-PBE (PBE0) [13] provide smaller overall MAEs in comparison with the corresponding pure functionals: 16.50 and 14.95 eV, respectively. For core orbitals, the OS global hybrid functionals based on BLYP and PBE also provide significantly small MAEs, which are slightly larger than those of SVWN5. The  $\alpha_i$  values determined by the GGA functionals are slightly smaller than those of SVWN5 and are significantly larger than the corresponding HFX portions used in B3LYP and PBE0. It is interesting that the MAEs exhibit relatively large changes although the changes in  $\alpha_i$  are significantly less.

Let us discuss the meta-GGA functional, TPSS. The MAEs decrease from the GGA and LDA functionals approximately by 10 and 17 eV for C1 orbitals and by 6 and 3 eV for C2 orbitals. The widely used hybrid version of TPSS (TPSSh) [71] exhibits a better performance against TPSS but yields a larger MAE in comparison with B3LYP and PBE0. By determining  $\alpha_i$  through the LCOE, MAEs are reduced, especially for core orbitals: 1.86 from 67.93 eV and 2.11 from 23.07 eV for C1 and C2 orbitals. The determined  $\alpha_i$  slightly but gradually decreases as ingredients such as the density gradient and the kinetic density are more involved. The values of  $\alpha_i$  for valence orbitals are larger than that of TPSSh.

The above assessment reveals that the LCOE improves FON dependence and estimation of IPs significantly for all global hybrid functionals, which bases SVWN5, BLYP, PBE, and TPSS XC functionals and an added HFX term. Finally, let us compare the results of the OS functional based on LC-BLYP. For core orbitals, the global hybrid-based OS functionals basically perform slightly better than the OS functional of LC-BLYP does, although the obtained  $\alpha_i$  values are relatively different. For valence orbitals, all OS functionals provide MAEs less than 0.5 eV. The MAE of the conventional LC-BLYP is the smallest among all functionals, which is consistent with the previous reports [100, 101]. The overall MAEs of the OS functional of LC-BLYP are comparable to those of the LDA, GGA, and meta-GGA functionals.

### 14.5.3 Brief Summary

We have constructed and assessed the OS global hybrid functionals satisfying the LCOE for core and valence orbitals. As was reported for LC hybrid functionals [53], the LCOE drastically reduces the FON dependence and enables accurate estimates

of IPs for not only core but also valence orbitals for HFx + DFTxc such as LDA, GGA, and meta-GGA. This numerical assessment leads to the conclusion that the LCOE is generally effective for constructing XC functionals.

The valence's OS HFx portions obtained for global hybrid functionals are significantly larger than those for LC hybrid functionals [53], although the core's ones are similar to those of LC hybrid functionals. The effect of HFx has been discussed theoretically and numerically from various points of view.

## 14.6 General Conclusions

The descriptions of core-ionized and core-excited states by DFT and TDDFT were discussed in this chapter. The core orbitals are significantly difficult to describe by conventional DFT methods because the core electron distribution, which is more localized than that of valence electron, leads to significant SIE. The numerical assessment on HFx contributions capable of reducing SIE motivated us to develop the new hybrid functional, CV-B3LYP, which selects the appropriate HFx portions for core and valence electrons for second-row elements. Although this chapter focuses on core orbital, an extension of CV-B3LYP to Rydberg orbitals is also demonstrated and succeeded in reproducing accurate core and valence excitations as well as Rydberg excitations [51]. The determination of HFx portions using a physical constraint, LCOE, was also explored and is promising for constructing XC functionals.

Core orbitals seem to attract more attention in connection with free-electron laser (FEL). The appearance of FEL, which has been developed in the world, may open a new science field: FEL has enabled to produce laser pulses strong enough to fully ionize molecules in short-wavelength regime [104]. The high intensity of FEL also enables to determine molecular structures without crystallization [105–107] and create multiply ionized and excited states involving core ionizations and core excitations [36, 104, 108]. These FEL experiments, however, do not provide the detailed information for specifying all processes including as the intermediate ones in the multiple photoionization processes. Theoretical analysis is required for analyzing chemical and physical phenomena caused by FEL. We believe that the improvement of description for core orbitals definitely enhances progress of the FEL science.

## References

1. Hohenberg P, Kohn W (1964) *Phys Rev* 136:B864
2. Kohn W, Sham LJ (1965) *Phys Rev* 140:A1133
3. Parr RG, Yang W (1989) *Density functional theory of atoms and molecules*. Oxford University Press, New York

4. Dreizler RM, Gross EKV (1990) Density functional theory. Springer, Berlin
5. Slater JC (1951) Phys Rev 81:385
6. Vosko SH, Wilk L, Nusair M (1980) Can J Phys 58:1200
7. Becke AD (1998) Phys Rev A 38:3098
8. Lee C, Yang W, Parr RG (1988) Phys Rev B 37:785
9. Perdew JP, Ernzerhof M, Burke K (1996) Phys Rev Lett 77:3865; *ibid.* (1997) 78: 1396 (E)
10. Tao JM, Perdew JP, Staroverov VN, Scuseria GE (2003) Phys Rev Lett 91:146401
11. Becke AD (1997) Phys Rev A 38:3098
12. Stephens PJ, Devlin FJ, Chabalowski CF, Frisch MJ (1994) J Phys Chem 98:11623
13. Adamo C, Barone V (1999) J Chem Phys 110:6158
14. Savin A (1996) In: Seminario JM (ed) Recent developments and applications of modern density functional theory. Elsevier, Amsterdam
15. Tawada Y, Tsuneda T, Yanagisawa S, Yanai T, Hirao K (2004) J Chem Phys 120:8425
16. Song JW, Hirotsawa T, Tsuneda T, Hirao K (2007) J Chem Phys 126:154105
17. Vydrov OA, Scuseria GE (2006) J Chem Phys 125:234109
18. Heyd J, Scuseria GE (2004) J Chem Phys 121:1187
19. Grimme S (2006) J Comput Chem 27:1787
20. Andersson Y, Langreth DC, Lundqvist BI (1996) Phys Rev Lett 76:102
21. Dobson JF, Dinte BP (1996) Phys Rev Lett 76:1780
22. Sato T, Nakai H (2009) J Chem Phys 131:224104
23. Becke AD, Johnson ER (2005) J Chem Phys 122:154104
24. Runge E, Gross EKV (1985) Phys Rev Lett 52:997
25. Casida ME (1995) In: Chong DP (ed) Recent advances in density functional methods. Part I. World Scientific, Singapore
26. Bauernschmitt R, Ahlrichs R (1996) Chem Phys Lett 256:454
27. Stratmann RE, Scuseria GE, Frisch MJ (1998) J Chem Phys 109:8218
28. Hirata S, Head-Gordon M (1999) Chem Phys Lett 314:291
29. Dreuw A, Weisman JL, Head-Gordon M (2003) J Chem Phys 119:2943
30. Casida ME, Salahub DR (2000) J Chem Phys 113:8918
31. Schirmer J, Cederbaum LS, Walter O (1983) Phys Rev A 28:1237
32. Cederbaum LS, Schleyer PVR, Schreiner PR, Allinger NA, Clark T, Gasteiger J, Kollman P (1998) In: Schaefer HF III (ed) Encyclopedia of computational chemistry. Wiley, New York
33. Ortiz JV (1988) J Chem Phys 89:6348
34. Kuramoto K, Ehara M, Nakatsuji H (2005) J Chem Phys 122:014304
35. Shirai S, Yamamoto S, Hyodo S (2004) J Chem Phys 121:7586
36. Tashiro M, Ehara M, Fukuzawa H, Ueda K, Buth C, Kryzhevoi NV, Cederbaum LS (2010) J Chem Phys 132:184302
37. Besley NA, Asmuruf FA (2010) Phys Chem Chem Phys 12:12024
38. Williams AR, deGroot RA, Sommers CB (1975) J Chem Phys 63:628
39. Slater JC (1972) Adv Quantum Chem 6:1
40. Chong DP, Hu C-H (1996) Chem Phys Lett 262:729
41. Chong DP (1995) Chem Phys Lett 232:486
42. Triguero L, Plashkevych O, Pettersson LGM, Agren H (1999) J Elect Spectrosc Relat Phenom 104:195
43. Gilbert ATB, Besley NA, Gill PMW (2008) J Phys Chem A 112:13164
44. Besley NA, Gilbert ATB, Gill PMW (2009) J Chem Phys 130:124308
45. van Leeuwen R, Baerends EJ (1994) Phys Rev A 49:2421
46. Imamura Y, Otsuka T, Nakai H (2007) J Comput Chem 28:2067
47. Imamura Y, Nakai H (2007) Int J Quantum Chem 107:23
48. Imamura Y, Nakai H (2006) Chem Phys Lett 419:297
49. Tsuchimochi T, Kobayashi M, Nakata A, Imamura Y, Nakai H (2008) J Comput Chem 29:2311
50. Nakata A, Imamura Y, Otsuka T, Nakai H (2006) J Chem Phys 124:094105
51. Nakata A, Imamura Y, Nakai H (2006) J Chem Phys 125:064109



52. Nakata A, Imamura Y, Nakai H (2007) *J Chem Theory Comput* 3:1295
53. Imamura Y, Kobayashi R, Nakai H (2011) *J Chem Phys* 134:124113
54. Imamura Y, Kobayashi R, Nakai H (2011) *Chem Phys Lett* 513:130
55. Imamura Y, Kobayashi R, Nakai H (to be Submitted)
56. Imamura Y, Kobayashi R, Nakai H. *Int J Quantum Chem* (Accepted)
57. Stener M, Decleva P (2000) *J Chem Phys* 112:10871
58. Stener M, Decleva P, Goerling A (2001) *J Chem Phys* 114:7816
59. Besley NA, Peach MJG, Tozer DJ (2009) *Phys Chem Chem Phys* 11:10350
60. Song J-W, Watson MA, Nakata A, Hirao K (2008) *J Chem Phys* 129:184113
61. Song J-W, Watson MA, Hirao K (2009) *J Chem Phys* 131:144108
62. Nakata A, Tsuneda T, Hirao K (2010) *J Phys Chem A* 114:8521
63. Perdew JP, Zunger A (1981) *Phys Rev B* 23:5048
64. Becke AD (1993) *J Chem Phys* 98:1372
65. Dunning TH Jr (1989) *J Chem Phys* 90:1007
66. Woon DE, Dunning TH Jr (1995) *J Chem Phys* 103:4572
67. Dunning TH Jr, Hay P (1977) In: Schaefer HF III (ed) *Methods of electronic structure theory*, vol 3. Plenum Press, New York
68. Frisch MJ, Trucks GW, Schlegel HB, Scuseria GE, Robb MA, Cheeseman JR, Montgomery JA Jr, Vreven T, Kudin KN, Burant JC, Millam JM, Iyengar SS, Tomasi J, Barone V, Mennucci B, Cossi M, Scalmani G, Rega N, Petersson GA, Nakatsuji H, Hada M, Ehara M, Toyota K, Fukuda R, Hasegawa J, Ishida M, Nakajima T, Honda Y, Kitao O, Nakai H, Klene M, Li X, Knox JE, Hratchian HP, Cross JB, Bakken V, Adamo C, Jaramillo J, Gomperts R, Stratmann RE, Yazyev O, Austin AJ, Cammi R, Pomelli C, Ochterski JW, Ayala PY, Morokuma K, Voth GA, Salvador P, Dannenberg JJ, Zakrzewski VG, Dapprich S, Daniels AD, Strain MC, Farkas O, Malick DK, Rabuck AD, Raghavachari K, Foresman JB, Ortiz JV, Cui Q, Baboul AG, Clifford S, Cioslowski J, Stefanov BB, Liu G, Liashenko A, Piskorz P, Komaromi I, Martin RL, Fox DJ, Keith T, Al-Laham MA, Peng CY, Nanayakkara A, Challacombe M, Gill PMW, Johnson B, Chen W, Wong MW, Gonzalez C, Pople JA (2004) *GAUSSIAN 03*, Revision C.02. Gaussian Inc., Wallingford CT
69. Domke M, Xue C, Puschmann A, Mandel T, Hudson E, Shirley DA, Kaindl G (1990) *Chem Phys Lett* 173:122
70. Hitchcock AP, Brion CE (1980) *J Elect Spectrosc Relat Phenom* 18:1
71. Staroverov VN, Scuseria GE, Tao J, Perdew JP (2003) *J Chem Phys* 119:12129
72. Roothaan CCJ (1960) *Revs Modern Phys* 32:179
73. Huzinaga S (1980) *Bunshikidouhou*. Iwanami Shoten, Tokyo (in Japanese)
74. Hirao K, Nakatsuji H (1973) *J Chem Phys* 59:1457
75. Schmidt MW, Baldrige KK, Boatz JA, Elbert ST, Gordon MS, Jensen JH, Koseki S, Matsunaga N, Nguyen KA, Su S, Windus TL, Dupuis M, Montgomery JA (1993) *J Comput Chem* 14:1347
76. Curtiss LA, Raghavachari K, Redfern PC, Pople JA (1997) *J Chem Phys* 106:1063
77. The basis set is obtained through the following site: <https://bse.pnl.gov/bse/portal>
78. Chong DP, Gritsenko OV, Baerends EJ (2002) *J Chem Phys* 116:1760
79. Ohno M, Decleva P, Fronzoni G (1998) *J Chem Phys* 109:10180
80. Dressler R, Allan M (1987) *J Chem Phys* 87:4510
81. Walker IC, Abuain TM, Palmer MH, Beveridge AJ (1988) *Chem Phys* 119:193
82. Serrano-Andrés L, Merchán M, Nebot-Gil I, Lindh R, Roos BO (1993) *J Chem Phys* 98:3151
83. Nakajima T, Hirao K (1999) *Chem Phys Lett* 302:383
84. Bodeur S, Millié P, Nenner I (1990) *Phys Rev A* 41:252
85. Cavell RG, Jürgensen AJ (1999) *J Elect Spectrosc Relat Phenom* 101–103:125
86. Bodeur S, Esteva JM (1985) *Chem Phys* 100:415
87. Bodeur S, Maréchal JL, Reynaud C, Bazin D, Nenner I, *Phys Z* (1990) *D-Atom Mol Clust* 17:291
88. Gedat E, Püttner R, Domke M, Kaindl G (1998) *J Chem Phys* 109:4471
89. Segala M, Takahata Y, Chong DP (2006) *J Elect Spectrosc Relat Phenom* 151:9

90. Robin MB (1975) *Chem Phys Lett* 31:140
91. Nayandin O, Kukk E, Wills AA, Langer B, Bozek JD, Canton-Rogan S, Wiedenhoef M, Cubaynes D, Berrah N (2001) *Phys Rev A* 63:062719
92. Itoh U, Toyoshima Y, Onuki H (1986) *J Chem Phys* 85:4867
93. Robin MB (1974) Chapter III. In: Higher excited states of polyatomic molecules, vol I. Academic, New York/London
94. Huber KP, Herzberg G (1979) *Molecular spectra and molecular structure IV. Constants of diatomic molecules*. Van Nostrand Reinhold, New York
95. Mori-Sánchez P, Cohen AJ, Yang W (2006) *J Chem Phys* 125:201102
96. Cohen AJ, Mori-Sánchez P, Yang W (2007) *J Chem Phys* 126:191109
97. Cohen AJ, Mori-Sánchez P, Yang W (2008) *Phys Rev B* 77:115123
98. Vydrov OA, Scuseria GE, Perdew JP (2007) *J Chem Phys* 126:1541091
99. Livshits E, Baer R (2007) *Phys Chem Chem Phys* 9:2932
100. Salzner U, Baer R (2009) *J Chem Phys* 131:231101
101. Tsuneda T, Song J-W, Suzuki S, Hirao K (2010) *J Chem Phys* 133:174101
102. Janak JF (1978) *Phys Rev B* 18:7165
103. Almbladh C-O, von Barth U (1985) *Phys Rev B* 31:3231
104. Young L, Kanter EP, Krässig B, Li Y, March AM, Pratt ST, Santra R, Southworth SH, Rohringer N, DiMauro LF, Doumy G, Roedig CA, Berrah N, Fang L, Hoener M, Bucksbaum PH, Cryan JP, Ghimire S, Glowia JM, Reis DA, Bozek JD, Bostedt C, Messerschmidt M (2010) *Nature* 466:56
105. Neutze R, Wouts R, van der Spoel D, Weckert E, Hajdu J (2000) *Nature* 406:752
106. Chapman HN et al (2011) *Nature* 470:73
107. Seibert MM et al (2011) *Nature* 470:78
108. Imamura Y, Hatsui T (2011) *Phys Rev A* 85:012524